Crustal-scale balanced cross-section and restorations of the Central Pyrenean belt (Nestes-Cinca transect): Highlighting the structural control of Variscan belt and Permian-Mesozoic rift systems on mountain building

Nicolas Espurt, P. Angrand, A. Teixell, P Labaume, M. Ford, Michel de Saint Blanquat, S. Chevrot

Crustal-scale balanced cross section and restorations of the Central Pyrenean belt (Nestes-Cinca transect): highlighting the structural control of Variscan belt and Permian-Mesozoic rift systems on mountain building

N. Espurt[1], P. Angrand[2], A. Teixell[3], P. Labaume[4], M. Ford[5], M. de Saint Blanquat[2], S. Chevrot[2]

[1]Aix Marseille Univ, CNRS, IRD, INRA, Coll France, CEREGE, Aix-en-Provence, France.

[2]Observatoire Midi Pyrénées, GET, CNRS UMR 5563, Université Paul Sabatier, Toulouse, France.

[3]Dept. de Geologia, Universitat Autònoma de Barcelona, 08193 Bellaterra, Spain.

[4]Géosciences Montpellier, Université de Montpellier-CNRS, 34095 Montpellier, France.

[5]CRPG, UMR 7358, Nancy, France.

Corresponding author: Nicolas Espurt (espurt@cerege.fr)

Abstract

In this paper, we combined new field geological, structural, paleo-temperature and subsurface data together with deep geophysical data to build a new 210 km-long crustal-scale balanced and sequentially restored cross section in the Central Pyrenean belt (Nestes-Cinca transect). The present-day surficial thrust system geometry of the belt consists of bi-vergent basement-cover thrust sheets with inverted extensional basins and halokinetic structures. Its crustal geometry consists of a thrust wedge geometry of the European lithosphere between the Axial Zone imbricate system of the Iberian upper crust and the north-directed subduction of the Iberian lower crust. Along the study transect, the contractional belt corresponds to the inversion of the Mesozoic Pyrenean Rift system, which consisted in a hyper-extended relay

zone of two metamorphic zones with exhumation of lithospheric mantle, the Montillet and Baronnies zones, separated by the Barousse upper crustal boudin. Surface and subsurface data show that the European and Iberian crusts include major inherited structures of the Variscan belt and Permian Rift. These old crustal features controlled the location and geometry of the Mesozoic Pyrenean Rift system. During the upper Cretaceous-lower Miocene contraction, both Paleozoic and Mesozoic inherited features controlled the thrust kinematics and the structural architecture of the Pyrenean orogen. Palinspastic restorations show that the orogenic shortening recorded in the Central Pyrenean belt reaches 127 km (39%) including the closure of the hyper-extended Pyrenean Rift system that initially archived 56 km of extension. This study emphasizes the long-term influence of Paleozoic-Mesozoic structural and thermal inheritances for the evolution of orogenic belts.

Keywords: Balanced cross section; Structural inheritance; Rifting; Variscan features; Central Pyrenean belt

1. Introduction

The Pyrenees result from the subduction of the Iberian lower crust and lithospheric mantle under the European plate from late Cretaceous to early Miocene (Muñoz, 1992; Olivet, 1996; Teixell et al., 2018; Chevrot et al., 2018, and references therein). Numerous studies showed that this orogen was superimposed on a Mesozoic magma-poor hyper-extended rift, the Pyrenean Rift system, with coeval HT-LP metamorphism and exhumation of the lithospheric mantle (e.g., Duée et al., 1984; Specht, 1989; Vielzeuf and Kornprobst, 1989; Golberg and Leyreloup, 1990; Lagabrielle and Bodinier, 2008; Jammes et al., 2009; Lagabrielle et al., 2010; Vacherat et al., 2014; Corre et al., 2016). The accommodation of more than 80 km of shortening through the inversion of this rift system is considered as the prime control to explain the present-day structural architecture of the Pyrenean orogen (Roure

et al., 1989; Specht, 1989; Muñoz, 1992; Vergés et al., 1995; Teixell, 1998; Beaumont et al., 2000; Vergés and García-Senz, 2001; Martínez-Peña and Casas-Sainz, 2003; Mouthereau et al., 2014; Teixell et al., 2016; Clerc et al., 2016; Grool et al., 2018; Teixell et al., 2018). The influence of inherited Paleozoic structures has been described in many Cenozoic fold-thrust belts worldwide such as the Andes (Colletta et al., 1997; Alvarez-Marron et al., 2006; Vergés et al., 2007; Espurt et al., 2008; Calderon et al., 2017), the Alps (Roure and Colletta, 1996; Jourdon et al., 2014; Ballèvre et al., 2018) and the Provence (Bestani et al., 2016). Although Paleozoic structures are well established in the Pyrenean orogen (Bresson, 1903; Muller and Roger, 1977; Lucas, 1985; Choukroune et al., 1990a,b; Desegaulx et al., 1990; Souquet et al., 2003; Saura and Teixell, 2006; García-Sansegundo et al., 2011; Cochelin et al., 2017; and references therein), the influence of these latter on Pyrenean geodynamics is poorly quantified and probably underestimated along the orogen (Muñoz, 1992; Specht, 1989; Cochelin et al., 2017). To illustrate the role of Paleozoic structural inheritances on the Mesozoic-Cenozoic geodynamic evolution of the Central Pyrenean belt, we combined new field geological, structural, paleo-temperature and subsurface data together with deep geophysical data. These data have been combined with cross section balancing methodology to constrain the structural architecture of the whole orogen along a crustal-scale, 210 km-long cross section following the Nestes and Cinca valleys (Fig. 1). A simplified version of this section was previously presented in Teixell et al. (2018) without restoration. This balanced cross section is strategically localized in a segment of the Pyrenean chain where both the Pyrenean and pre-Pyrenean deformations can be studied. It follows the trace of the OROGEN West profile (Chevrot et al., 2018) illustrating the deep geometry of the pre-Mesozoic basement framework involved in this collisional orogen (Fig. 1). Comparison between present-day crustal geometry and three sequentially retro-deformed stages (lower Santonian, upper Jurassic and lower-middle Triassic) of this section shows that the Pyrenees was superimposed on a complex

structural template affected by the Variscan orogeny and subsequent Permian Rift, that in turn controlled subsequently the geometry of the Mesozoic rift and the building of the upper Cretaceous-lower Miocene Pyrenean orogen. This example from the Central Pyrenees reveals the long-term influence of inherited tectonic crustal fabric in the evolution of orogenic belts.

2. Geological setting

2.1. Tectonic framework of the Pyrenean belt

The Pyrenean belt is an asymmetrical bi-vergent collisional orogen. The orogen is divided from north to south into five structural domains: the Aquitaine Basin, the North Pyrenean Zone, the Axial Zone, the South Pyrenean Zone and the Ebro Basin (Fig. 1). The Aquitaine Basin is poorly deformed by deep-seated faults and diapiric structures (James and Canérot, 1999; Rocher et al., 2000; Canérot et al., 2005; Serrano et al., 2006). The North Pyrenean Zone wedge comprises a system of Mesozoic extensional basins including HT-LP metamorphism pre-rift and syn-rift sedimentary units, basement structures and lherzolite bodies (Ravier, 1957; Albarède and Michard-Vitrac, 1978; Montigny et al., 1986; Azambre et al., 1991; Clerc et al., 2016). These basins are now inverted and transported southward and northward above the Axial Zone and the Aquitaine Basin along the former rift borders, the North Pyrenean Frontal Thrust to the north and the North Pyrenean Fault Zone to the south (Baby et al., 1988; Roure et al., 1989; Debroas, 1990; Ford et al., 2016; Teixell et al., 2016, 2018). The southern wedge comprises the south-verging antiformal stack of the Axial Zone made of Iberian Variscan basement comprising a Paleozoic metasedimentary succession and upper Paleozoic granitoid intrusions. Southward, Mesozoic and Tertiary cover units of the South Pyrenean Zone are detached from the Axial Zone over an upper Triassic evaporite and shale unit (Séguret, 1972; Muñoz et al., 1986). The South Pyrenean Zone comprises Mesozoic inherited extensional faults and related halokinetic structures, thrust faults and syn-orogenic

thrust-sheet-top basins of late Santonian to early Miocene age. It displays a complex along-strike structure controlled by the distribution of Triassic evaporites and thickness variations of the Mesozoic strata, resulting in sub-basins separated by oblique thrust zones with vertical axis rotations (Soto et al., 2002; Mochales et al., 2012; Muñoz et al., 2013; López-Mir et al., 2014b; Santolaria et al., 2016). The South Pyrenean Zone overrides the mildly deformed Ebro Basin along the South Pyrenean Frontal Thrust (Puigdefàbregas, 1975; Puigdefàbregas and Souquet, 1986).

Field data, paleogeographic reconstructions and crustal-scale sections across the Pyrenees show that the Iberian-European plate boundary was affected by superimposed tectonic events (e.g., Lucas, 1968, 1985; Debroas, 1987; Roure et al., 1989; Coward and Dietrich, 1989; Mattauer 1990; Choukroune et al., 1990a; Muñoz, 1992; Teixell, 1998; Sibuet et al., 2004; Gong et al., 2009; García-Sansegundo et al., 2011). Although debated, the Variscan orogeny in the Pyrenees is characterized by different deformation phases in a contractional to transpressional geodynamic setting featuring, metamorphism, magmatism and syn-orogenic sedimentation (e.g., Soula, 1982; Soula et al., 1986; Deselgaulx et al., 1990; Carreras and Cappellà, 1994; García-Sansegundo et al., 2011; Cochelin et al., 2017). The shortening in the Variscan belt was accommodated by major S-verging thrust sheets with mid-crustal and Silurian graphitic slates detachment levels associated with E-W trending right-lateral strike-slip fault system located between the European and Iberian plates, and NE-SW trending cross faults such as the Toulouse fault (Arthaud and Matte, 1975; Soula et al., 1986; Burg et al., 1990; Choukroune et al., 1990a; Souquet et al., 2003; Fig. 1). During the Permian to lower Triassic breakup of Pangea and middle Triassic to middle Cretaceous opening of the Atlantic Ocean, transtensional to N-S extensional motions resulted in stretching and thinning of the continental crust, and development of sedimentary depocenters and crustal blocks

between the Iberian and European plates (Vissers, 1992; Jammes et al., 2009; Tugend et al., 2015; Tavani et al., 2018; Asti et al., 2019).

2.2. Stratigraphy

The lithostratigraphic units across the Central Pyrenees along the Nestes-Cinca transect are summarized in Fig. 2 and described hereafter. In the northern Pyrenees, the sedimentary rocks are named after the PYRAMID ANR project stratigraphic nomenclature (Ford et al., 2016; Rougier et al., 2016).

2.2.1. Variscan basement rocks and Permian-Triassic red beds

Paleozoic rocks outcrop in the North Pyrenean Zone (Barousse massif) and Axial Zone (Fig. 3). They consist of Cambrian-Ordovician metasediments, Silurian graphitic slates, Devonian-lower Carboniferous limestones and pelites, and upper Carboniferous syn-orogenic siliceous and carbonaceous turbidites (the so-called Culm facies) deformed during the Variscan orogeny (Roddaz, 1977; Zwart, 1986; Delvolvé, 1987; Mirouse et al., 1993). In the Aquitaine Basin, undifferentiated Paleozoic rocks were found in the LNZ2 well as a rock body within upper Triassic sediments and at the bottom of the AC2 well (Fig. 1 and Supplementary material Fig. S1). Paleozoic sequences are intruded by syn- to post-orogenic upper Carboniferous granitoids (Bordères-Louron, Néouvielle and Bielsa; Gleizes et al., 2001; Román-Berdiel et al., 2004; Gleizes et al., 2006) and Permian granitoids (Sarrancolin and Ferrère; Harris, 1976). During Permian (uppermost Carboniferous?) rifting, continental breccia beds deposited in NNE-SSW to ESE-WNW trending intracontinental basins like the Aure trough (Lucas, 1985). The Paleozoic framework has been eroded and unconformably covered by widespread lower-middle Triassic fluvial deposits including conglomerates, sandstones and argillites (Buntsandstein facies; Calvet et al., 2004). The thickness of these

143 Permian-Triassic red beds varies from 120 m or less in the Barousse massif to more than 1.5
144 km into the Aure trough (Lucas, 1968; Flachère, 1977; Mirouse et al., 1993; Fig. 3).

145 2.2.2. Middle Triassic-lower Aptian evaporitic to marine succession

146 The Triassic red beds are overlain by middle Triassic carbonates (Muschelkalk facies)
147 and upper Triassic evaporites and shales (Keuper facies) successions deposited during the
148 opening of the Bay of Biscay. Upper Triassic strata contain doleritic-ophitic sill and dyke
149 bodies (Curnelle, 1983). Liassic to lower Aptian strata consist of dominantly marine to
150 platform carbonate strata (Barrère et al., 1984). In the study area, Berriasian strata are
151 unconformably covered by Urgonian-Barremian limestones. Although these carbonate
152 sequences are considered to be deposited during the post-rift stage, Hettangian, Kimmeridgian
153 and Tithonian strata show major thickness and facies variations with volcanic levels,
154 evaporitic sequences, and sedimentary breccias (Fig. 4a; Delfaud, 1966, 1968; Barrère et al.,
155 1984; James et al., 1996; Fauré, 2002; Canérot et al., 2005; Biteau et al., 2006; Rougier et al.,
156 2016). Breccia intercalations are also reported in Berriasian and Barremian strata (Delfaud,
157 1966, 1968; Barrère et al., 1984). Thickness and facies changes in Jurassic and lower
158 Cretaceous sequences could be due to salt motion synchronous with basement extension.

159 2.2.3. Upper Aptian-lower Cenomanian Pyrenean Rift succession

160 The subsequent development of the Pyrenean Rift system at the eastern termination of
161 the Bay of Biscay is associated with upper Aptian to lower Cenomanian thick turbiditic
162 deposits (Black Flysch Group), fringed by platform carbonates (Urgonian facies) during the
163 early stages (Paris and Icole, 1975; Souquet et al., 1985; Debroas, 1990; Ternet et al., 1995;
164 Figs. 4b,c,d). In the Baronnies zone, the Black Flysch Group is locally associated with chaotic
165 breccias of pre-rift Mesozoic and basement rocks (Debroas, 1990). Near the North Pyrenean
166 Fault Zone, upper Albian-Cenomanian limestones of Sarrancolin display breccia intervals

made up of centimetric to metric clasts of Cretaceous limestones and older rocks (Jurassic metasediments, upper Triassic dolerites, Permian-Triassic red beds and Ordovician schists; Barrère et al., 1984; Ternet et al., 1995; Figs. 4e,f). The Mesozoic rocks of the North Pyrenean Zone were affected by HT-LP metamorphism (peak temperatures from 250 to 500°C), attested by the presence of scapolite in Jurassic and Cretaceous limestones, and include locally serpentinized lherzolite bodies as in Avezac region (Choukroune, 1972; Azambre et al., 1991; Barrère et al., 1984; Vacherat et al., 2014; Figs. 3 and 4c,d).

In the South Pyrenean Zone of the Cinca valley, the upper Triassic strata are overlain by sparsely preserved Jurassic limestones and marls, and thin lower Cretaceous-Cenomanian conglomerates, sandstones and mudstones under unconformable upper Cretaceous strata (López-Mir et al., 2014b and references therein).

2.2.4. Turonian-lower Santonian rift- to post-rift succession

Thick Turonian-lower Santonian turbidite successions (Grey Flysch Group) of the North Pyrenean Zone and Aquitaine Basin were deposited during the thermal cooling phase following the Aptian-Cenomanian rifting (Ford et al., 2016). These sediments pinch out to the north in the Aquitaine Basin. To the south, the strata onlap onto the Permian-Triassic red beds or Variscan basement in the Axial Zone. Near the North Pyrenean Fault Zone, Turonian-Coniacian (lower Santonian?) calcareous turdidites and calcschists contain breccia intervals comprising clasts of Mesozoic carbonates, Ordovician schists and granite (Barrère et al., 1984; Ternet et al., 1995). South of the Axial Zone, the lower part of the late Cretaceous is dominantly composed of platform limestones. In the Cotiella thrust sheet of the South Pyrenean Zone, the middle Coniacian-lower Santonian post-rift succession recorded spectacular extensional salt tectonic structures, due to northward gravity sliding along the Iberian Platform (García-Senz, 2002; McClay et al., 2004; López-Mir et al., 2014b).

2.2.5. Upper Cretaceous-Cenozoic syn- to post-orogenic succession

Upper Santonian-Maastrichtian deposits record the onset of the Pyrenean shortening. These deposits infill E-W trending turbidite troughs developed in the northern and southern forelands of the Pyrenees. In the northern Pyrenees, the syn-orogenic succession corresponds to Campanian-Maastrichtian marine turbidites supplied from the east in an external platform (Petites Pyrénées Group) to open marine environment in the southern Aquitaine Basin (Vacherat et al., 2017). In the southern Pyrenees, the upper Santonian Campo Breccia records the onset of inversion of the Cotiella basin (Garrido-Megías, 1973; García-Senz, 2002). Southwards and upwards, the breccia grades into the turbiditic system of the Vallcarga Formation, and subsequently into shelf to transitional sandstone of the Areny Formation (Garrido-Mejías, 1973; Puigdefàbregas and Souquet, 1986; García-Senz, 2002; López-Mir et al., 2014b).

In the northern Pyrenees, the overlying Paleocene-Eocene strata have marine (Rieubach Group to the west) to non-marine detrital and carbonate facies (Aude Valley Group to the east, Garumnian facies), followed by the marine carbonate succession of the Coustouge Group. The uppermost fluvial and lacustrine Carcassonne Group (upper Eocene-Oligocene) was sourced from the uplifting orogen to the south (Christophoul et al., 2003; Ford et al., 2016; Rougier et al., 2016).

In the southern Pyrenees, the Paleocene-Eocene syn-orogenic strata correspond to basal transgressive shallow marine limestones, which backstep to the south, overlain by the deep-water marls and turbidites of the Ainsa Basin (Mutti et al., 1985; Puigdefàbregas and Souquet, 1986). They are fed from the east by the fluvial to deltaic sandstone and conglomerate systems of the Tremp-Graus basin. The Ainsa Basin is then filled by the prograding middle-upper Eocene Sobrarbe deltaic complex comprising conglomerates,

sandstones and mudstones grading into terrestrial red beds (Escanilla Formation) (Garrido-Megías and Ríos-Aragües, 1972; Dreyer et al., 1999). Growth folding and compressional salt tectonics have been recorded by Paleocene-Eocene strata (Garrido-Mejías, 1973; Teixell and Barnolas, 1995; Poblet et al., 1998; Muñoz et al., 2013; Santolaria et al., 2016).

Along the South Pyrenean Frontal Thrust, the northern edge of the Ebro Basin is filled by upper Priabonian to lower Rupelian alluvial systems that pass laterally to the south to playa-lake evaporites (Barbastro Gypsum Formation). These are overlain by coarse-grained Oligocene-Miocene fluvial to alluvial siliciclastic sediments (Crusafont et al., 1966; Quirantes, 1969; Riba et al., 1983). Miocene clastic sediments often overlap and bury the South Pyrenean Frontal Thrust, which is poorly emergent in the study transect (Fig. 1).

Post-orogenic alluvial deposits (Miocene-Pliocene) of the Lannemezan megafan cover a large area in the Aquitaine Basin (Hubschman, 1975; Mouchené et al., 2017). The megafan is characterized by many Quaternary terrace staircases related to incision by the Neste River.

2.2.6. Mechanical stratigraphy and décollement levels

The structure of the Axial Zone is controlled by décollement levels in the Cambrian-Ordovician basement and Silurian graphitic slates (Desegaulx et al., 1990; Muñoz, 1992). Basement thrusts branch upward into upper décollements developed in the upper Triassic evaporite-shale strata and/or upper Cretaceous carbonates (Séguret, 1972; Desegaulx et al., 1990; Vergés et al., 1992; Teixell et al., 2000; Cámara and Flinch, 2017). Shallower décollement levels are observed in the Eocene shales and southern evaporite sequences in the South Pyrenean Zone and northern Ebro Basin (Flachère, 1977; Santolaria et al., 2016).

During the Permian and Mesozoic extensions, Silurian graphitic slates and upper Triassic evaporites also acted as decoupling levels between upper extensional structures in the

cover and lower crustal detachment faults (Jammes et al., 2010a; Clec and Lagabrielle, 2014; Manatschal et al., 2015; Asti et al., 2019).

3. Datasets

In this study, we use new field observations and structural data mainly from the North Pyrenean Zone and Axial Zone, 1:50 000 BRGM (Bureau de Recherches Géologiques et Minières) and IGME (Instituto Geológico y Minero de España) geologic maps, subsurface data, and previously published deep geophysical data to build a 210 km-long crustal-scale cross section (Fig. 1). From north to south, the section crosses the Aquitaine Basin along the ~76 km long LR06 seismic reflection profile (Fig. 5), the North Pyrenean Zone and the Axial Zone along the Nestes valley, the South Pyrenean Zone along the Cinca valley and reaches the northern edge of the Ebro Basin. The LR06 seismic reflection profile has been depth-converted using well data (see Supplementary material Table S1) and reinterpreted from Serrano et al. (2006). The bottom of the profile reaches 18 km depth and has been interpreted using eleven exploration wells (see Supplementary material Fig. S1), the bottom of the deeper well reaching 6.9 km bsl under the Lannemezan area (Fig. 5). We have also used the shallow sections constructed by Lucas (1985) and Debroas (1990) in the North Pyrenean Zone, sections by Román-Berdiel et al. (2004) and Jolivet et al. (2007) in the Axial Zone, sections by López-Mir et al. (2014b), Teixell and Barnolas (1995), Cámara and Flinch (2017) and Santolaria et al. (2016) in the South Pyrenean Zone, and the upper crustal cross section of Martínez-Peña and Casas-Sainz (2003). Finally, the section follows the trace of the OROGEN West receiver function profile (Chevrot et al., 2018; Fig. 1), referred to as the PYROPE Center profile in Teixell et al. (2018).

New Raman spectroscopy of carbonaceous material (RSCM) data in the North Pyrenean Zone (Table 1) are integrated into the restoration as well as published Raman data

obtained in the North Pyrenean Zone (Ducoux, 2017), apatite fission track data obtained in granitoids and metamorphic rocks of the Axial Zone and North Pyrenean Zone (Morris et al., 1998; Fitzgerald et al., 1999; Jolivet et al., 2007; Labaume et al., 2016a; Mouchené, 2016).

4. Surface and subsurface structural architecture

In the following, we describe the structural architecture of the section from north to south.

4.1. The Aquitaine Basin

The geology and geometry of the Aquitaine Basin has been widely studied for hydrocarbon exploration (Bourrouilh et al., 1995; Le Vot et al., 1996; Biteau et al., 2006; Serrano et al., 2006; Serrano, 2015). In the Aquitaine Basin, the surface geology is masked by Miocene-Pliocene deposits of the Lannemezan megafan and Quaternary alluvium (Fig. 3). The North Pyrenean Frontal Thrust is a major north-verging thrust exposed along the North Pyrenean chain, transporting the North Pyrenean Zone above the Aquitaine Basin (Souquet et al., 1977). Subsurface data show that numerous deep-seated structures are hidden under the Aquitaine Basin sediments north of the North Pyrenean Frontal Thrust (e.g., Rocher et al., 2000; Serrano et al., 2006). The interpretation of the LR06 seismic reflection profile (Fig. 5) indicates that the structure of the Aquitaine Basin is mainly related to basement-involved structures associated with shallower compressional and halokinetic structures in the sedimentary cover (Gensac-Bonrepos, Auzas-Saint Médard and Auch; Serrano et al., 2006). Although the reflectors are of poor quality at depth, we interpreted the Paleozoic basement of the Aquitaine Basin as deformed by a set of north-dipping normal faults, delimiting half grabens filled by Permian (uppermost Carboniferous?) strata (Fig. 5). Some normal faults were reactivated as normal faults during the Mesozoic, then as thrusts during the Pyrenean compression (Auzas-Saint Médard and Auch structures). These basement faults may

correspond to inherited south-verging Variscan thrusts as described along the ECORS Pyrenees profile further east (Roure et al., 1989; Choukroune et al., 1990a,b). Southward, the sedimentary cover is deformed by the North Pyrenean Frontal Thrust, which consists in two branches: the lower North Pyrenean Frontal Thrust, a tectonic wedge detached northward in upper Triassic evaporites, involving two major diapiric structures (the shallower Gensac-Bonrepos to the north and a deeper salt structures to the south) and a deep tectonic slice under the North Pyrenean Zone interpreted as the western continuation of the Saint-Gaudens dense body; the upper North Pyrenean Frontal Thrust, a complex north-verging imbricate system involving Paleozoic, Triassic and lower Cretaceous rocks as revealed by well data (Fig. 5 and Supplementary material Fig. S1; Paris and Icole, 1975; Serrano et al., 2006). The upper North Pyrenean Frontal Thrust transported the Baronnies zone onto Paleocene strata of the Aquitaine Basin; the thrust displacement is sealed by upper Eocene strata.

4.2. The North Pyrenean Zone

In the Nestes valley, the North Pyrenean Zone is divided into two metamorphic zones, the Baronnies and Montillet zones, separated by the Barousse Paleozoic massif (Figs. 3 and 6a; Choukroune, 1971; Barrère et al., 1984; Debroas, 1990). In these metamorphic zones, the Mesozoic rocks are affected by middle Cretaceous (ca. 110-90 Ma) HT-LP metamorphism contemporaneous with polyphase syn-extensional/compressional ductile deformations (Fig. 4; Henry et al., 1971; Choukroune, 1972; Debroas, 1990; Azambre et al., 1991) as described in the Chaînon Béarnais (Teixell et al., 2016).

In the northern Baronnies metamorphic zone (the so-called external metamorphic zone), Urgonian limestones, Albian-Cenomanian breccias and flysch are folded in the Bourg, Prat and Bazus synclines (Fig. 7). These synclines are bounded by steep south-verging thrusts including tectonic slices of Urgonian limestones, Triassic rocks and small bodies of

serpentinized lherzolite as along the Avezac thrust (Figs. 4c and 7; Debroas, 1990; Azambre et al., 1991). To the south, the Bazus syncline and Estivère anticline show preserved, tilted or inverted Mesozoic normal faults (such as the Mazouau and Estivère faults; Fig. 8a,b) probably rooted at depth into the Triassic evaporites. The Estivère fault was transported southward above the Lechan thrust (Figs. 7 and 8b). This thrust cuts with a shortcut geometry through the Jurassic-lower Cretaceous cover of the Barousse massif (Pène Haute unit).

The Barousse massif is an E-W trending, 30 km long and ~4 km-wide amygdale-shaped basement unit of highly deformed Ordovician to Devonian schists and limestones with Permian granitic intrusions, unconformably covered by Mesozoic strata of the Bassia and Pène Haute units (Figs. 3 and 7; De Villechenous, 1980). The cross-sectional geometry of the Barousse massif corresponds to an asymmetric antiform underlined by lower Triassic red beds (Lucas, 1968). The backlimb dips 30-40° northward while the forelimb is vertical to overturned along the Barricave fault zone (Fig. 7).

South of the Barricave fault zone, the southern Montillet metamorphic zone (the so-called internal metamorphic zone) is characterized by two narrow synclines (Montillet and Beyrède) with steep and sheared limbs (Lucas, 1968; Barrère et al., 1984). These synclines are bounded by steep faults including tectonic slices (Pariou and Houle Verte) of Ordovician schists and Triassic red beds and dolomites, dolerite, and marble (Figs. 3, 4e and 8c). The northern Montillet syncline is composed of Jurassic metamorphic dolomites and limestones and Albian flysch in the fold core. This syncline disappears progressively westward under low grade metamorphosed Mesozoic strata of the Bassia unit (Fig. 3). The Montillet syncline is transported southward over the inverted limb of the Beyrède syncline above the 70° north-dipping Castet thrust. The Beyrède syncline folds upper Albian-Cenomanian limestones and breccias and Turonian-Coniacian flysch (Barrère et al., 1984; Figs. 3, 7 and 8c). These rocks were intensively sheared during extensional and compressional tectonics with polyphase

335 folding (Fig. 4f,h; Henry et al., 1971; Choukroune, 1972). The Beyrède syncline is bounded to
336 the south by the Beyrède fault. This fault zone appears as a 67° north-dipping thrust
337 emplacing the North Pyrenean Zone over Triassic 45° north-dipping strata of the northern
338 Axial Zone (Figs. 7, 8c,d and 9a). The Castet and Beyrède thrusts define the southern border
339 of the North Pyrenean Zone as portions of the North Pyrenean Fault Zone.

340 4.3. The Axial Zone

341 In the Central Pyrenees, the Axial Zone is formed by five south-verging thrust sheets
342 (Arreau, Gavarnie, Millares, Bielsa, and Guarga) dominantly made of crystalline and
343 metamorphic basement and Paleozoic meta-sedimentary rocks covered by small remnants of
344 Permian-Triassic and Cretaceous strata (Figs. 3 and 7; Muñoz, 1992; Martínez-Peña and
345 Casas-Sainz, 2003; Jolivet et al., 2007). Tectonic transport of these basements units during the
346 Pyrenean compression is clearly attested by Triassic and Cretaceous strata in the footwall of
347 the thrusts (Fig. 3). The northernmost Arreau thrust unit is mainly composed of highly
348 deformed and foliated Carboniferous turbidites and limestones unconformably overlain by the
349 80° to 45° north-dipping Permian-Triassic red beds of the Aure trough (Lucas, 1968; 1985;
350 Mirouse et al., 1993; Figs. 6a, 7 and 8d). Southward, the footwall of the Arreau thrust shows
351 thin Triassic red beds dipping 30° to 80° northward (Fig. 9b) which unconformably overlie
352 granite and Devonian-Carboniferous strata of the Gavarnie unit (Lucas 1985; Gleizes et al.,
353 2006; Fig. 3). Upper Paleozoic strata of the Gavarnie thrust unit are deformed by major folds
354 with strong cleavage together with thrusting (i.e., Cadéac, Ancizan and Vielle-Aure thrust
355 systems; Figs. 3, 6a and 10a,b) interpreted as Variscan deformations (Bresson, 1903; Muller
356 and Roger, 1977; Mirouse et al., 1993). Field data and previous works suggest that these
357 structures have been weakly reactivated during the Mesozoic rifting and Pyrenean
358 compression (Bresson, 1903; Mirouse et al., 1993; Gleizes et al., 2006). The Gavarnie thrust
359 dips ~40° north below Silurian slates (Fig. 10c). Its displacement is here estimated up to 10

km (Séguret, 1972; Martínez-Peña and Casas-Sainz, 2003; Jolivet et al., 2007). This thrust loses displacement toward the east and eventually disappears (e.g., Soler et al., 1998; Cochelin et al., 2017; Teixell et al., 2018). In the footwall of the Gavarnie thrust, the Millares thrust unit is mainly composed of metamorphic Cambro-Ordovician rocks (Frédancon dome), Silurian-Devonian strata to the southeast and remnants of unconformable Permian-Triassic red beds and upper Cretaceous limestones (Fig. 3; Clin et al., 1989; Mirouse et al., 1993). Field data and previous retrodeformed cross sections restoring the Pyrenean shortening suggest internal Variscan folding and thrusting in the Millares unit (Martínez-Peña and Casas-Sainz, 2003; Román-Berdiel et al., 2004). The Millares thrust dips ~20° to the north, becoming flat to the south as indicated by klippes of Devonian limestones of the Millares thrust unit above Permian-Triassic red beds of the Bielsa unit (Figs. 3 and 6a). These klippes argue for 4.5 km of minimum displacement on the Millares thrust above the Bielsa unit. The Bielsa thrust unit is dominantly formed by Variscan granite unconformably overlain by Permian-Triassic red beds. These latter are flat to the north and dip ~40° southward to the south (Fig. 6a). The basement thrust sheets described above were deformed and transported southward onto the deep Guarga basement thrust unit below the Ainsa Basin (Figs 6a,b; Cámara and Klimowitz, 1985).

4.4. The South Pyrenean Zone and Ebro Basin

The South Pyrenean Zone is composed of a south-verging imbricate fan of thrust sheets of Mesozoic to Oligocene cover rocks (Séguret, 1972; Garrido-Megías, 1973; Fig. 6b) detached in upper Triassic evaporites. Along the Cinca valley, these thrust sheets and associated folds record a large clockwise vertical axis rotation above lateral ramps (e.g., Mochales et al., 2012; Muñoz et al., 2013). From north to south, the thrust sheets are the Cotiella, Peña Montañesa, Boltaña-Balzes, and Sierras Marginales thrust sheets (Fig. 6b; García-Senz, 2002; Muñoz et al., 2013; López-Mir et al., 2014b; Santolaria et al., 2014). The

Cotiella thrust sheet corresponds to a spectacular inverted gravity-driven salt-based extensional rollover basin formed during Turonian-early Santonian times (López-Mir et al., 2014a,b). Now, this thrust sheet appears as an isolated klippe transported to the south from the Axial Zone (Séguret, 1972), implying a minimum southward displacement of 20 km (López-Mir et al., 2014a). The Ainsa Basin in the footwall of the Cotiella and Peña Montañesa thrust sheets is filled by Eocene turbidite to deltaic deposits deformed by the La Fueba or Arro fold-thrust system (Fig. 6b; Barnolas et al., 1991; Fernández et al. 2012; Muñoz et al., 2013). Southward, the Clamosa and Naval Triassic salt domes rose during the Eocene and Oligocene and, together with internal thrusts, are transported in the hanging-wall of the Boltaña-Balzes thrust (Teixell and Barnolas, 1995; Muñoz et al., 2013; Santolaria et al., 2014; Cámara and Flinch, 2017). Based on the gravity modeling results of Santolaria et al. (2016), we infer a deep south-verging thrust (accommodating ~5.5 km of shortening) made of the Eocene rocks under the Clamosa diapir to fill space and thus decrease the volume of the Triassic evaporites (Fig. 6b). Southward, the Sierras Marginales structure corresponds to a single south-verging thrust sheet of the upper Cretaceous to Eocene strata defining the South Pyrenean Frontal Thrust above the Barbastro-Balaguer ridge (Cámara and Klimowitz, 1985; Santolaria et al., 2016). As previously mentioned, the frontal thrust is poorly emergent as it is largely buried by Miocene sediments on this transect. The Barbastro-Balaguer ridge is a detachment anticline made of Oligocene-Miocene molasse with Eocene evaporitic sediments in its core (Fig. 6a; Martínez-Peña and Pocoví, 1988; Cámara and Flinch, 2017).

5. Paleo-temperature data

Raman spectroscopy on carbonaceous material (Beyssac et al., 2002; Lahfid et al., 2010) is used to determine the maximum paleo-temperatures that affected the North Pyrenean Zone rocks. These maximum paleo-temperatures provide an estimation of the paleo-burial in order to constrain the restored pre-deformational basin architecture. Maximum paleo-

410 temperatures were determined for eight carbonaceous samples in the North Pyrenean Zone
411 along the studied transect. Maximum paleo-temperatures obtained range from 274 to 556°C
412 (Figs. 3 and 7, and Table 1) and are consistent with data of Ducoux (2007). Higher values
413 (~500°C) are found in the center of the external and internal metamorphic zones (Baronnies
414 and Montillet zones) for samples collected in Jurassic and Albian-Cenomanian limestones and
415 breccias. Lower values (~300°C) are found in the Estivère anticline (southern edge of the
416 Baronnies zone) and Beyrède syncline for samples collected in Albian to Turonian limestones
417 and breccias.

418 **6. Timing of thrust propagation**

419 In the Aquitaine Basin, thrust activity is mainly recorded by Campanian to Eocene
420 deposits with growth strata patterns controlled by the Gensac-Bonrepos, Auzas-Saint Médard
421 and Auch anticlines (Fig. 5). Thrust activity and exhumation of the North Pyrenean Zone are
422 only constrained as middle-late Eocene (between 41.8 and 35.1 Ma) by apatite fission track
423 cooling ages in the granitoids of Barousse massif (Mouchené, 2015) and in anatectic
424 paragneisses west of the Baronnies zone (Labaume et al., 2016b). In the Axial Zone, timing of
425 thrust-related uplifts occurred between the late Eocene and the early Miocene as suggested by
426 apatite fission track cooling ages in granitoids belonging to the Gavarnie and Bielsa thrust
427 sheets (Morris et al., 1998; Fitzgerald et al., 1999; Jolivet et al., 2007; Labaume et al., 2016b).
428 In the South Pyrenean Zone, syn-tectonic breccias and growth strata record the activity of the
429 Cotiella thrust sheet during the late Santonian (Campo unconformity and breccias; Figs. 2 and
430 6b) and late Maastrichtian, the Peña Montañesa thrust sheet during the Paleocene-late
431 Ypresian, and the Boltaña-Balzes and Sierras Marginales thrust sheets during Lutetian-
432 Oligocene (García-Senz, 2002; Muñoz et al., 2013; López-Mir et al., 2014b; Santolaria et al.,
433 2014; Labaume et al., 2016a). Thrust propagation occurred synchronously with lower
434 Lutetian to upper Bartonian clockwise vertical axis rotation that was also accommodated by

local steeply-dipping normal cross faults (e.g., San Marcial graben in Fig. 6b; Mochales et al., 2012; Muñoz et al., 2013; López-Mir et al., 2014b; Santolaria et al., 2014).

7. Crustal-scale balanced cross section and restorations

The crustal structure of the Central Pyrenean belt is derived from the update interpretation of receiver function data of the coincident OROGEN West profile (Chevrot et al., 2018) shown in Fig. 11, together with gravity anomaly data (International Gravimetric Bureau, 2012) and gravity inversion results of Casas et al. (1997). The final balanced and restored cross sections are shown in Fig. 12. This balanced cross section is one possible construction model but the most reasonable solution consistent with the available surface and subsurface geological data presented in this study.

Cross section balancing follows thrust tectonic concepts (Dahlstrom, 1969; Boyer and Elliot, 1982; Elliott, 1983). Balancing and restorations were performed using Move structural modeling software based on bed length and thickness conservation and the built-in flexural-slip algorithm for the sedimentary cover. An area-balance approach was applied for the deep crustal levels (Mitra and Namson, 1989). The Triassic evaporite layer was not balanced during restoration because this layer is considered free to move in three dimensions and to be eroded in successive stages of exposed diapirism. The large difference of volume of the Triassic evaporites between the present-day and restored stages can also result from major dissolution and fluid migration.

Fault and basin geometries, facies distribution, and burial data allow us to reconstruct three palinspastic restorations: early Santonian, late Jurassic and early-middle Triassic. Taking the associated sedimentary sequences as markers (with respect to the depth of deposition at regional-scale), sequential restoration allows the modeling of the geometry of the Pyrenean Rift system during middle Cretaceous and late Jurassic, and Permian Rift-

Variscan belt. Lower-middle Triassic and Jurassic markers are preserved along the section. Because the lower Santonian markers have been eroded in the North Pyrenean Zone, Raman paleo-temperature data are used to estimate the paleo-thickness of the pre-orogenic sedimentary pile. The lower Santonian pre-contractional restoration quantifies the amount of Pyrenean shortening while the lower-middle Triassic restoration estimates the Mesozoic extension. The calculated extension and shortening magnitudes that we propose are minimum values owing to the uncertainty involved in calculating the amount of thrust displacement where hanging wall cut-offs are removed by erosion (see Judge and Allmendinger, 2011 for discussion). In addition, we assume that strike-slip motions inferred at least along the North Pyrenean Fault Zone and rotations in the South Pyrenean Zone would not significantly affect the structural geometry. However, they may affect the estimated amount of shortening or extension (e.g., Wallace, 2008).

7.1. Present-day crustal-scale geometry

The surficial thrust system geometry of the Central Pyrenean belt consists in bi-vergent basement and cover thrust sheets with the inversion of extensional faults and diapiric structures. The asymmetry of the belt is defined by a wide (~126 km) south-verging prowedge including the northern part of the Ebro Basin, the South Pyrenean Zone, the Axial Zone, the Montillet zone and the Barousse massif, and a relatively narrower (~73 km) north-verging retrowedge including the Baronnies zone and the deformed Aquitaine Basin (Fig. 12a).

The crustal structure of the Central Pyrenean belt section is similar to the one described to the east along the ECORS Pyrenees and PYROPE East profiles (Fig. 1; Chevrot et al., 2015; Teixell et al., 2018; Chevrot et al., 2018). The European lithosphere constitutes a thrust wedge indenting southward between the upper crustal Axial Zone imbricate stack and the northward subducted Iberian lowermost crust. The European crust exhibits a wedge-

shaped geometry thinning southward from ~30 km-thick in the north to zero km-thick under the Axial Zone. In contrast, the Iberian crust shows a regular thickness of ~32 km between the Ebro Basin and the Axial Zone. The profile is marked by the presence of a wave-shaped negative polarity interface, which mimics the north-dipping Iberian Moho (Chevrot et al., 2018). These interfaces describe a boudinaged 30-15 km-thick, ~20° north-dipping slab of Iberian lower crust plunging into the mantle to a depth of ~75 km under the Aquitaine Basin (Fig. 11).

The Iberian crust shows a strong internal complexity with an intriguing northward gently dipping negative polarity (Fig. 11). This interface is located at a depth of 15 km bsl under the South-Pyrenean Zone. It connects northward with the subducting lower crust under the Axial Zone. This interface is also visible along-strike in the PYROPE West and East profiles (Chevrot et al., 2018). We speculate that this inclined interface is a relic of a major south-verging Variscan thrust, detached in the lower crust. Additional deeper thrusts might also occur southward. This crustal imbricate feature is consistent with Paleozoic basement reflectors in the ECORS Pyrenees profile interpreted as Variscan flats and ramps by Choukroune et al. (1990a,b) and Desegaulx et al. (1990). The large negative polarity in the European crust (Fig. 11) is rather interpreted as a multiple of the shallow sediment layer of the Aquitaine Basin (Chevrot et al., 2018). Like for the Iberian crust, we assume that the Variscan basement thrusts of the European crust under the Aquitaine Basin are also connected at depth into the lower crust (Choukroune et al., 1990a,b).

Following the North Pyrenean Zone in map view, a series of relatively strong positive Bouguer anomalies (Saint-Gaudens, Lourdes, Labourd) are aligned parallel to the trend of the chain (Casas et al., 1997; Angrand et al., 2018; Chevrot et al., 2018; Fig. 11). These anomalies have been interpreted as dense material (either lower crust or mantle) exhumed during Cretaceous rifting then transported northward by Pyrenean thrusts onto European

upper crust (e.g., Roure et al., 1989; Muñoz, 1992; Casas et al., 1997). Our section crosses the western edge of the Saint-Gaudens dense body (Figs. 11 and 12a). The location and size of this dense body is constrained by gravity data (International Gravimetric Bureau, 2012) and consistent with the modeling results of Casas et al. (1997). We represented this dense body (with an area of ~85 km² at a depth ranging between 8.5 and 16 km bsl) as a sheared thrust lense of mantle rock thrust along the deep North Pyrenean Frontal Thrust (Fig. 12). Our construction shows that the Saint-Gaudens body is tectonically overlain by basement thrust sheets of the Axial Zone and underlain by European upper crust. Alternatively, the western Labourd anomaly is interpreted as an autochthonous uplifted upper mantle below thinned European crust that was only passively transported along a south-verging thrust (Velasque et al., 1989; Wang et al., 2016). This more recent model seems, however, poorly constrained in terms of kinematics and accommodation of observed surface shortening, as discussed by Teixell et al. (2018).

7.2. Lower Santonian pre-contractional restoration

The lower Santonian restored cross section (Figs. 12b and 13) shows the structural architecture of the Pyrenean Rift system just before the onset of the Pyrenean compression. The rift forms a 75 km-wide asymmetric hyper-extended zone with a central basement unit (the Barousse massif) surrounded by the ~20 km-wide northern metamorphic zone (Baronnies zone), and the ~50 km-wide southern metamorphic zone (Montillet zone) with high grades of HT-LP metamorphism. Relative vertical positions and burial of the sedimentary units have been estimated according to peak paleo-temperatures of ~270-550°C indicated by Raman data (Fig. 13) and consistent with diagenesis/metamorphism data of Azambre et al. (1991) in the Baronnies zone. These paleo-temperatures and the reconstructed paleo-depths of the sedimentary/tectonic units indicate maximum geothermal gradient values ranging between 75 and 110°C/km (considering a deep-sea temperature of ~20°C) before the upper Santonian

533 inversion. This is also consistent with the geothermal gradient of ~80°C/km calculated from
534 zircon helium data in the Mauléon Basin further west (Vacherat et al., 2014; Hart et al., 2017;
535 Fig. 1).

536 At the transition zone between the European Platform and Baronnies zone, the
537 Jurassic-Cretaceous sedimentary cover is detached toward the south above huge volume of
538 Triassic evaporitic related to the development of large halokinetic structures (area of the
539 future lower North Pyrenean Frontal Thrust; Fig. 13). The northern edge of the Baronnies
540 zone is formed by a major listric south-dipping normal fault corresponding to the future upper
541 North Pyrenean Frontal Thrust. The Baronnies zone is restored to show a 5.5 km-thick
542 depocenter mainly constituted by Albian-Cenomanian (and inferred Turonian-lower
543 Santonian) strata deformed by north- and south-dipping low-angle normal faults associated
544 with diapirism and extensional raft structures above upper Triassic evaporites like in the
545 Chaînons Béarnais basins (Canérot and Lenoble, 1991, 1993; Lagabrielle et al., 2010; Jammes
546 et al., 2010a; Teixell et al., 2016; Corre et al., 2016; Fig. 1). In the center of the Baronnies
547 zone, the Cretaceous sediments tectonically overlie exhumed mantle rocks (Fig. 13). The
548 Barousse massif is detached from the distal Iberian margin above the future north-dipping
549 North Pyrenean Fault Zone (Castet and Beyrède normal faults). We propose that the structure
550 of the Barousse massif can be modeled as an upper crustal boudin (its nature is however
551 poorly constrained at depth) on which its Mesozoic sedimentary cover (Pène Haute and
552 Bassia) has been detached to slide northward above Triassic evaporites into the Baronnies
553 zone (Fig. 13). Southward, the subsidence of the Montillet zone is controlled by normal slip
554 above the Beyrède and Castet basement faults and also by gravitational sliding of the cover
555 above Triassic evaporites (Barricave fault zone). This extensional system is covered by thick
556 (more than 5 km-thick) Albian to Coniacian (lower Santonian?) sediments. In the Iberian
557 Platform, the evolution of Cotiella Basin during the middle Coniacian-early Santonian was

558 controlled by gravity-driven extension and diapirism (Fig. 13; López-Mir et al., 2014a,b). The
559 gravitational sliding is probably favored by northward tilting of the Triassic basal décollement
560 and differential sediment loading during the post-rift period.

561 The restored geometry of the Cretaceous Pyrenean Rift system shows that extreme
562 thinning and stretching of the crust resulted in the exhumation of the subcontinental mantle
563 under the Baronnies zone (Avezac lherzolite) and probably also under the Montillet zone.
564 Although the southern Montillet metamorphic zone is devoid of peridotite rocks, it could be
565 connected to the east to the well-known Lherz area (Aulus Basin; Fig. 1) where remnants of
566 exhumed mantle are well preserved (e.g., Lagabrielle and Bodinier, 2008). The stretching of
567 the crust is heterogeneous in the rift axis with crustal thinning and boudinage leading to upper
568 crustal rocks (e.g., Barousse boudin) and Cretaceous sediments lying directly over the mantle
569 (Clerc and Lagabrielle, 2014). The restoration shows that the thick sedimentary cover is
570 continuous without exposures of exhumed mantle rocks at the seabed, a situation
571 corresponding to the T-type lherzolite exhumation process described by Lagabrielle et al.
572 (2010). The origin of the small lherzolite bodies along the Avezac thrust is not clear in their
573 present context of small tectonic lenses (Figs. 3 and 4c). They can be interpreted as mantle
574 fragments embedded in Triassic evaporites during extension and later collected by thrusting
575 during the Pyrenean inversion (Lagabrielle et al., 2010; Teixell et al., 2016).

576 The restoration indicates that extensional faulting and exhumation of the metamorphic
577 units continued at least during the Turonian-Coniacian, which is consistent with breccia
578 deposits with basement and Jurassic clasts near the North Pyrenean Fault Zone and
579 burial/metamorphic peak in the rift (Montigny et al., 1986; Azambre et al., 1991). A similar
580 interpretation for the end rifting age was proposed for the northeastern Pyrenean section in
581 Clerc et al. (2016).

582 Our restoration of the Pyrenean Rift system shows many similarities with the ductile-
583 type magma-poor rifted margin model including boudinage of the lower crust and ductile
584 deformation of the upper crust just beneath the sedimentary cover as described in Clerc and
585 Lagabrielle (2014) and Clerc et al. (2018). Our restoration suggests that HT-LP
586 metamorphism in the cover of the Baronnies and Montillet zones is related to deep burial
587 (more than 5 km-thick) coupled with crustal thinning and mantle exhumation (Golberg and
588 Leyreloup 1990; Clerc and Lagabrielle, 2014; Clerc et al., 2016).

589 Our two-dimensional restoration and field data suggest a partitioned hyper-extended
590 rift system in this sector of the Pyrenean Rift system (Figs. 12b and 13). This sector can be
591 interpreted as the relay zone between the southern internal metamorphic zone mainly
592 developed eastward along the North Pyrenean Fault Zone (i.e., Montillet, Ballongue and
593 Aulus basins) and the northern external metamorphic zone mainly developed westward (i.e.,
594 Baronnies, Chaînons Béarnais and Mauléon basins) (Fig. 1; Jammes et al., 2010b; Lagabrielle
595 et al., 2010; Tugend et al., 2014; Masini et al., 2014; Teixell et al., 2016; Corre et al., 2016).
596 This structural model is consistent with the non-cylindrical geometry of the Cretaceous basins
597 (V-shaped geometries), separated by crustal boudins as proposed by Jammes et al. (2009) and
598 Clerc and Lagabrielle (2014).

599 7.3. Upper Jurassic restoration

600 The upper Jurassic restored cross section (Fig. 14b) suggests that the region would
601 have already suffered crustal extension and halokinesis during middle Triassic-Jurassic in a
602 ~100 km-wide zone localized north of the Castet fault including the European Platform
603 (future Auzas-Saint Médard structure). We propose that the extension is accommodated at
604 depth by faulted basement blocks and low-angle detachments in the upper crust with inferred
605 thinning by ductile shear in the lower crust. In the zone of maximum crustal thinning (i.e., the

606 zone of the future Pyrenean Rift system), the mobility of Triassic evaporites could have been
607 enhanced by high geothermal gradient. According to field data, the restoration suggests
608 gravitational sliding of the Jurassic cover above Triassic evaporites (Fig. 14b) with the
609 development of several salt-related anticlines and growth synclines like in the Chaînons
610 Béarnais (Fig. 1; Canérot and Lenoble, 1991, 1993;). The huge volume of Triassic evaporites
611 may have favored canopy emplacements as suggested by the development of evaporitic
612 sequences in Jurassic (Delfaud, 1968; Barrère et al., 1984; Fauré, 2002). This Jurassic
613 tectonic/halokinesis activity is also consistent with breccia deposition at least during the
614 Hettangian, Kimmeridgian and Tithonian (Delfaud, 1966, 1968; Barrère et al., 1984; James et
615 al., 1996; Fauré, 2002). Jurassic sequences deposited on the Iberian margin have been
616 strongly eroded and are only preserved south of the Bielsa unit. Although the European and
617 Iberian rift shoulders show thick Triassic evaporitic sequences, these zones are only affected
618 by minor halokinetic movements, may be due to the smaller thermal effect in these zones.

619 7.4. Lower-middle Triassic restoration

620 The lower-middle Triassic restoration of Fig. 14c illustrates a possible crustal
621 architecture model before the Mesozoic rifting events. The restoration suggests that the
622 Central Pyrenean orogen was superimposed on an irregular Paleozoic framework including
623 Variscan compressional and Permian extensional structures. The restored Guarga, Millares,
624 Bielsa and Gavarnie unit can be interpreted as old Variscan thrusts according to geophysical
625 interpretations in the Iberian crust (Fig. 11). The Variscan thrust system is thus characterized
626 by several south-verging, ~15-20° north-dipping basement thrusts and synclines involving
627 Silurian to Carboniferous strata as described along the ECORS Pyrenees profile (Choukroune
628 et al., 1990a,b). The thrust system would be mainly detached in the lower crust. The thrusts
629 branch upward into décollements in the Silurian slates. The Barousse massif is interpreted as
630 an inherited Variscan south-verging thrust sheet. This thrust places Ordovician rocks onto

631 Carboniferous rocks of the Arreau syncline. The restoration also suggests that Ordovician
632 rocks of the Barousse thrust sheet are overlain to the north by a 3.5 km-thick package of
633 younger Paleozoic strata (Silurian, Carboniferous and Permian basins). These Paleozoic
634 sequences may connect northward with basement reflectors observed in the LR06 profiles in
635 the Aquitaine Basin (Fig. 5).

636 As described above, the restoration also suggests that some Variscan thrusts were
637 reactivated and controlled the formation of half-grabens during the Permian extension (Fig.
638 14c). The Aure trough (Lucas, 1968) corresponds to a large half-graben controlled by the
639 north-dipping Arreau normal fault on its southern border. Lucas (1968, 1985) showed that this
640 half-graben was infilled by thick continental breccia deposits (Fig. 8d) composed of locally
641 derived clasts mainly sourced from the Barousse massif to the north (Ordovician quartzite,
642 granite and slate) and from the Cadéac imbricate-Arreau basin to the south (Devonian
643 limestones, Carboniferous quartzites and limestones) (Fig. 3). This sediment provenance
644 suggests that the relative position of the different Variscan blocks across the future North
645 Pyrenean Fault Zone was not significantly modified along-strike since the Permian extension.
646 We emphasize that this model is consistent with results of Saspiturry et al. (2018) in the
647 Permian Bidarray Basin (Fig. 1). The Triassic restoration suggests thickness variations of the
648 crust along the section. The Permian Rift affecting the southern part of the European crust
649 may explain its relatively thinner lower crust (~15-23 km) in comparison to the Iberian crust
650 (~30 km), which was only weakly affected by crustal extension. This Permian crustal thinning
651 implies mantle uplift toward shallow lithosphere levels, which is consistent with post-
652 Variscan refertilization of the mantle lherzolites in the Aulus Basin (Lherz area; Le Roux et
653 al., 2007; Fig. 1) together with the development of Permian metasomatic events in the eastern
654 Pyrenees (Boutin et al., 2016). Variscan and Permian structures were eroded and

655 unconformably covered by fluvial Triassic strata mainly sourced from the north (Lucas, 1968,
656 1985).

657 7.5. Estimates of extension and shortening

658 The amount of crustal extension in the Pyrenean Rift system derived from crustal
659 restorations is 10 km at the end of late Jurassic and 56 km at the end of the early Santonian
660 (Fig. 14). This latter value is a minimum value because the restored southern Montillet
661 metamorphic zone may only represent a small remnant of a larger basin, now removed by
662 compression and erosion. Our estimate falls within the lower part of the ~70-50 km range
663 values estimated by Vergés and García-Senz (2001) from balanced cross sections and
664 Mouthereau et al. (2014) along the ECORS Pyrenees profile from plate kinematic models, and
665 consistent with thermo-mechanical modeling results of Jourdon et al. (2019).

666 The comparison between the present-day balanced and lower Santonian restored cross
667 sections shows a total horizontal shortening of 127 km (39%) accounting for the closure of the
668 hyper-extended Pyrenean Rift system in the Nestes-Cinca transect (Fig. 12). This value is a
669 minimum due to the uncertainties described above. This shortening is divided as 42 km in the
670 northern retrowedge (31 km for the Baronnies zone and 11 km for the Aquitaine Basin) and
671 85 km in the southern prowedge. The restoration shows that the shortening recorded by the
672 Axial Zone-Barousse imbricate has been totally accommodated upward in the emerging thrust
673 sheets of the South Pyrenean Zone and in the Barbastro-Balaguer ridge. The restoration
674 suggests that the 26 km of slip on the Cotiella-Peña Montañesa thrust sheets might have been
675 fed by the inversion of the North Pyrenean Fault Zone (15.1 km) and the rest by internal
676 south-verging thrusts of the Pyrenean Rift system (Fig. 12). In contrast to Martínez-Peña and
677 Casas-Sainz (2003), we propose a simple alternative root for the Cotiella thrust sheet here
678 placed above the Gavarnie unit (Teixell et al., 2018). The Arreau thrust can be interpreted as

679 an out-of-sequence thrust with a displacement of 3.5 km minimum. Further research on this
680 fault is needed to precise the geometry and inversion of the Permian-Triassic Aure trough
681 (Lucas, 1968).

682 The amount of shortening across the Pyrenean belt is debated. Shortening values in the
683 Central and Eastern Pyrenees estimated by balanced cross sections and paleogeographic
684 reconstructions range between 80 and 165 km (Roure et al., 1989; Muñoz, 1992; Vergés et al.,
685 1995; Teixell, 1998; Beaumont et al., 2000; Martínez-Peña and Casas-Sainz, 2003;
686 Mouthereau et al., 2014; Macchiavelli et al., 2017; Grool et al., 2018). Studies considering
687 and quantifying the closure of the exhumed mantle domain propose shortening amounts
688 ranging between 114 and 160 km (Specht, 1989; Mouthereau et al., 2014; Teixell et al., 2016;
689 Macchiavelli et al., 2017; Teixell et al., 2018), which is consistent with the calculated
690 shortening value of 127 km along the Nestes-Cinca transect of the Central Pyrenean belt.

691 **8. Discussion**

692 8.1. Influence of inherited Paleozoic features on Pyrenean geodynamics

693 The heterogeneous continental crust of the Pyrenees is inherited primarily from the
694 Variscan orogeny and the Permian rifting episode, including their relevant magmatic/thermal
695 events. These events resulted in substantial rheological changes in the lithosphere and the
696 individualization of crustal blocks separated by mechanical anisotropies (Manatschal et al.,
697 2015). However, the precise role of Paleozoic structural inheritances on Pyrenean
698 geodynamics remains poorly constrained.

699 The inferred lower-middle Triassic cross section restoration (Fig. 14c) suggests that
700 the Pyrenean domain is superimposed on a south-verging upper crustal thrust wedge of the
701 Variscan belt detached in the mid-lower crustal levels (Soula et al., 1986; Souquet et al.,

2003; García-Sansegundo et al., 2011). This inferred geometry is consistent to the one of the Variscan orogen of southwestern Iberia described in Simancas et al. (2001, 2003). Similarly, surface and subsurface data indicate that the upper crust is decoupled from the lower crust together with additional deformation occurring at deeper levels. Our structural model implies that lower crustal rocks may have been involved in Variscan thrusts in the Iberian margin as interpreted in the OROGEN West profile (Fig. 11). Thus, we can speculate, according to the restored geometry of the Variscan belt in Fig. 14c, that the basement thrusts of the present-day Axial Zone of Pyrenees as well as basement thrusts under the Aquitaine Basin might incorporate lower crustal rocks at depth (Fig. 12).

Variscan post-orogenic collapse is thought to have been responsible for Permian extensional reactivation of the pre-existing south-verging thrusts (Roure et al., 1989; Choukroune et al., 1990a,b), crustal thinning and the development of continental basins infilled by coarse detrital sedimentation from proximal relief (Lucas, 1985). Lower crustal rocks may have been exposed near the surface probably as early as the Permian, i.e., before the Cretaceous rifting (Vissers, 1992; Lagabrielle et al., 2016; Asti et al., 2019). The Paleozoic framework was eroded and then sealed by the lower Triassic red beds. During the middle Triassic-lower Santonian extensional period, the rift location and progressive necking of the continental lithosphere took place in a zone where the crust had been strongly deformed by the Variscan orogen, then thinned and newly intruded by granitoids during the Permian rifting (Harris et al., 1974). Comparison of lower Santonian, upper Jurassic and lower-middle Triassic restorations (Fig. 14) suggests that the inversion of the north-dipping Variscan Barousse thrust controlled the position of the southern edge of the Jurassic extension and Cretaceous Pyrenean Rift system, which then became the North Pyrenean Fault Zone. We propose that the northern edge of the rift might have been rather controlled by basement

726 tilting toward the rift and south-verging gravitational sliding of the Mesozoic cover above the
727 Triassic evaporites (Fig. 14a).

728 8.2. Inversion of the Pyrenean Rift system and building of the Pyrenees

729 During the closure of the Pyrenean Rift system, the exhumed mantle zone and the
730 Iberian lower crust were subducted underneath the European plate while the upper crust was
731 stacked as an internal zone of the Pyrenean orogen. The subduction of the hyper-extended
732 domain is associated with the reactivation of the North Pyrenean Fault Zone as a south-
733 verging thrust system. Shortening propagated southward with the initial inversion of the
734 Cotiella Basin in late Santonian (84 Ma), which coincides with the syn-tectonic Campo
735 breccia deposits and the development of flysch basins in the south Pyrenean domain attesting
736 onset of flexural subsidence (Garrido-Mejías, 1973; López-Mir et al., 2014a,b). Inversion is
737 recorded somewhat later in the northern Pyrenees by Campanian syn-orogenic flysch deposits
738 (Ford et al., 2016).

739 Numerical models suggest that the presence of mantle lithospheric bodies at shallow
740 depth in the retrowedge of the Pyrenees can be controlled by rifting inheritance (Jammes and
741 Huismans, 2012; Erdős et al., 2014; Jourdon et al., 2019). The thermal/structural inheritance
742 of the Cretaceous Pyrenean Rift domain was prone to accommodate the first crustal and cover
743 contractional deformations of the Pyrenean belt (Vacherat et al., 2014). The high geothermal
744 gradient caused by the hyperextension was probably maintained during at least early stages of
745 structural inversion in the Montillet and Baronnies zones (Fig. 4; Choukroune,1972; Debroas,
746 1990; Lacombe and Bellahsen, 2016). However, the exhumed mantle at upper crustal levels
747 acted as a rigid domain during the subsequent shortening (Jourdon et al., 2019). We propose a
748 kinematic model where the Saint-Gaudens mantle body is collected by thrusting during
749 inversion of the rift as suggested in the ECORS Pyrenees transect by Muñoz (1992) and in the

Chaînons Béarnais transect by Teixell et al. (2016) (Fig. 1). The reason why the mantle is alternately collected by thrust along the Pyrenean orogen remains unclear. Pyrenean thrusts could superimpose on inherited extensional shear zones of the exhumed mantle domain (Vissers et al., 1997; Gillard et al., 2016; Jourdon et al., 2019; Asti et al., 2019).

The transition from subduction to collision might correspond to the onset of subduction of the Iberian lower crust into the mantle (e.g., Teixell et al., 2016; Grool et al., 2018; Teixell et al., 2018). After, the European lithosphere acted as an intercutaneous wedge involving the decoupling of the Iberian crust in the ductile lower crust (Fig. 12). The timing of crustal accretion is difficult to estimate but it probably started synchronously with the growth of the imbricate stack and exhumation of the Axial Zone and North Pyrenean Zone at the end of the Eocene as suggested by apatite fission track cooling ages at ca. 42-35 Ma (Jolivet et al., 2007; Labaume et al., 2016b; Mouchené, 2016) and field geological data (Teixell, 1996; Labaume et al., 2016a).

The new crustal-scale balanced cross section and geophysical data argue in favor of a geodynamic model where the structure of the orogen is dominated by a south-directed large prowedge (Séguret, 1972; Muñoz et al., 1986). The shortening of the wedge was mainly transferred southward into cover thrust sheets of the South Pyrenean Zone which is consistent with numerical models of Erdős et al. (2014). The growth of the Axial Zone and North Pyrenean Zone mainly results from the piggyback-sequenced stacking of south-verging basement thrust sheets developed during the upper Cretaceous-lower Miocene Pyrenean compression (Séguret, 1972; Specht, 1989; Muñoz, 1992; Teixell, 1998). This kinematic propagation resulted in progressive and overall northward backtilting of the northern units (except in the northern edge of the Baronnies zone) and southward tilting of the southern units (Fig. 12).

774 8.3. Implication for Iberian kinematics

775 Although the European-Iberian plate boundary was affected by superimposed tectonic
776 events during the Mesozoic (e.g., Tugend et al., 2015; Macchiavelli et al., 2017), cross section
777 restoration results suggest that the relative position of the different Variscan blocks was not
778 significantly modified along-strike since the late Paleozoic times as was suggested in previous
779 studies (e.g., Lucas, 1968, 1985; Debroas, 1987; Coward and Dietrich, 1989; Roure et al.,
780 1989; Mattauer, 1990; Choukroune et al., 1990a,b; Muñoz, 1992; Sibuet et al., 2004; García-
781 Sansegundo et al., 2011; Tavani et al., 2018; Saspiturry et al., 2018). Although we cannot
782 provide new geometrical constraints to the relative plate motions, we propose that the opening
783 direction of the Pyrenean Rift system was mainly ~NNE-SSW trending since the Permian-
784 Triassic period and accommodated by major NNE-SSW trending transfer zones inherited
785 from the Paleozoic times like the Toulouse and Pamplona faults and Eastern Crustal
786 Lineament in the Pyrenees (Fig. 1; Tugend et al., 2015; Angrand et al., 2018; Cadenas et al.,
787 2018; Tavani et al., 2018), and the Nîmes and Durance faults and East-Variscan Shear Zone
788 in Provence basin (Bestani et al., 2016; Ballèvre et al., 2018; Tavani et al., 2018). However,
789 E-W trending intraplate transtensional deformations could be recorded southward in the
790 Iberian plate (Sibuet et al., 2004; Tugend et al., 2015; Rat et al., 2019). The structural
791 architecture of a rift system (sedimentary infill, width, symmetry of the conjugate margin pair
792 and underlying crustal properties) and its kinematics can abruptly change across crustal
793 transfer faults (Corti et al., 2003). Corre et al. (2016) argue that these transform faults also
794 participated to intense fluid circulations coeval with mantle exhumation and metamorphism in
795 the basins. Comparison of different cross sections and geophysical data between the Basque-
796 Cantabrian basin to the west and Provence basin to the east (Roca et al., 2011; Bestani et al.,
797 2016; Teixell et al., 2018 and references therein) suggests that these NNE-SSW trending
798 transfer faults controlled the along-strike structural changes and extension amount in the

Pyrenean Rift system, and then the present-day crustal architecture of the Pyrenees (Diaz et al., 2018; Chevrot et al., 2018).

9. Conclusions

The Pyrenees offer the exceptional opportunity to study the structural evolution of a belt and decipher the role of structural inheritance, which is generally impossible in orogens with large amounts of contractional deformation. In this study, we combined new field geological, structural, paleo-temperature and subsurface data together with deep geophysical data to build a 210 km-long crustal-scale cross section across the Central Pyrenean belt along the Nestes-Cinca transect. This study highlights the underestimated long-term influence of inherited Paleozoic tectonic structures in the evolution of Mesozoic and Cenozoic geological systems in Western Europe. The main conclusions are as follow:

1) The surficial thrust system geometry of the Central Pyrenean belt consists in bi-vergent basement and cover thrust sheets with the inversion of Mesozoic extensional basins and halokinetic structures. The crustal geometry consists in a thrust wedge geometry of the European lithosphere between the Axial Zone imbricate of the Iberian upper crust and the north-directed subduction of the Iberian lower crust. We confirm that the deep Saint-Gaudens gravity anomaly under the North Pyrenean Zone can be interpreted as a tectonic slice of mantle rocks that has been transported northward along the lower North Pyrenean Frontal Thrust.

2) In this sector of the Central Pyrenean belt, we showed that the Mesozoic Pyrenean Rift system consisted in an asymmetric hyper-extended relay zone of two metamorphic zones/basins, the northern metamorphic zone (Baronnies zone) and the southern metamorphic zone (Montillet zone), separated by the Barousse crustal boudin. The middle Triassic-early Santonian evolution of the Pyrenean Rift system was associated with brittle to ductile

deformation of the upper crust and cover together with gravitational sliding above Triassic evaporites and diapirism, and ductile thinning and stretching of the lower crustal levels. Extreme crustal thinning and stretching resulted in the exhumation of the subcontinental mantle coeval with deep burial and peak temperatures of ~550°C in metamorphic basins as indicated by Raman spectroscopy data.

3) The total horizontal orogenic shortening recorded in this zone of the Pyrenean belt is estimated to be at least 127 km (39%). This shortening value accounts for the closure of the Pyrenean Rift system, which itself achieved an estimated total crustal extension of 56 km minimum between the European and Iberian plates during Mesozoic times.

4) The Central Pyrenean belt was superimposed on a segment of the Variscan belt characterized by south-verging basement thrust sheets in the present-day European and Iberian crusts, and North Pyrenean Zone and Axial Zone. These structures were intermittently reactivated as normal faults during the Permian Rift, then controlled the location and kinematic of the Mesozoic Pyrenean Rift system. Finally, both Paleozoic and Mesozoic structural/thermal inheritances controlled the building of the Pyrenean orogen.

5) Finally, we infer that the opening of the Pyrenean Rift system was mainly NNE-SSW trending since the Permian-Triassic period and accommodated by transfer zones inherited from the Variscan period (e.g., Toulouse and Pamplona faults and Eastern Crustal Lineament). This could explain why the relative position of the different Variscan blocks was not significantly modified along-strike as suggested by our palinspastic restorations and previous studies. We propose that E-W trending intraplate transtensional deformations could be recorded southward in the Iberian plate in agreement with Tugend et al. (2015) and Rat et al. (2019).

Acknowledgments

847 This work was supported by the French National Research Agency PYRAMID project (Le
848 Nord des Pyrénées : évaluation intégrée de l'histoire de la Migration des fluides, l'Inversion du
849 rift, le rôle des processus de surface et la Déformation dans un (rétro)prisme orogénique) and
850 the BRGM-RGF (Bureau des Ressources Géologiques et Minières-Référentiel Géologique de
851 la France) Pyrénées program. The International Gravimetric Bureau (BGI) is acknowledged
852 for providing gravity data. Midland Valley is acknowledged for providing academic license of
853 Move for structural modeling. We thank S. Brusset, B. Roddaz, J.-C. Soula, F. Christophoul,
854 B. López-Mir, P. Santolaria, A. Casas and J. Canérot for helpful discussions. We
855 acknowledge Y. Lagabrielle, E. Masini and an anonymous reviewer for the exhaustive and
856 constructive comments which greatly helped us to improve the original manuscript.

857 **Appendix A. Supplementary material**

858 Supplementary material related to this article can be found on-line at…

859 **References**

860 Albarède, F., Michard-Vitrac, A. (1978). Age and significance of the North Pyrenean
861 metamorphism. Earth and Planetary Science Letters, 40, 327–332.

862 Alvarez-Marron, J., Rodriguez-Fernandez, R., Heredia, N., Busquets, P., Colombo, F.,
863 Brown, D. (2006). Neogene structures overprinting Palaeozoic thrust system in the
864 Andean Precordillera at 30°S latitude. Journal of Geological Society, 163, 949–964.
865 https://doi:10.1144/0016-76492005-142

866 Angrand, P., Ford, M., Watts, A. B. (2018). Lateral variations in foreland flexure of a rifted
867 continental margin: The Aquitaine Basin (SW France). Tectonics, 37.
868 https://doi.org/10.1002/2017TC004670

869 Arthaud, F., Matte, P. (1975). Les décrochements tardi-hercyniens du sud-ouest de l'Europe.
870 Géometrie et essai de reconstitution des conditions de la déformation. Tectonophysics,
871 25, 139–171. https://doi:10.1016/0040-1951(75)90014-1

872 Asti, R., Lagabrielle, Y., Fourcade, S., Corre, B., Monié, P. (2019). How do continents
873 deform during mantle exhumation? Insights from the northern Iberia inverted paleo-
874 passive margin, western Pyrenees (France). Tectonics, accepted.

875 Aurell, M., Meléndez, G. (2002). Jurassic: South Pyrenean basin. In: Gibbons, W. and
876 Moreno, M.T. (Eds.), The Geology of Spain. Geological Society, London, 221–233.

877 Azambre, B., Sagon, J. P., Debroas, E. J. (1991). Le métamorphisme crétacé du fossé des
878 Baronnies (Hautes-Pyrénées, France), témoin des anomalies thermiques de la zone
879 transformante nord-pyrénéenne. Comptes rendus de l'Académie des sciences. Série 2,
880 Mécanique, Physique, Chimie, Sciences de l'univers, Sciences de la Terre, 313(10),
881 1179-1185.

882 Baby, P., Crouzet, G., Specht, M., Deramond, J., Bilotte, M., Debroas, E.-J. (1988). Rôle des
883 paléostructures albo-cénomaniennes dans la géométrie des chevauchements frontaux
884 nord-pyrénéens. Comptes Rendus de l'Académie des Sciences de Paris Série II, 306,
885 307-313.

886 Barnolas, A., Samsó, J. M., Teixell, A., Tosquella, J., Zamorano, M. (1991). Evolución
887 sedimentaria entre la Cuenca de Graus-Tremp y la Cuenca de Jaca-Pamplona. In I
888 Congreso del Grupo Español del Terciario, Guide Book 1, 123 pp., F. Colombo, Vic,
889 Spain.

890 Ballèvre, M., Manzotti, P., Dal Piaz, G. V. (2018). Pre-Alpine (Variscan) inheritance: a key
891 for the location of the future Valaisan Basin (Western Alps). Tectonics, 37. https://doi-
892 org.insu.bib.cnrs.fr/10.1002/2017TC004633

893 Barrère, P., Bouquet, C., Debroas, E. J., Pélissonnier, H., Peybernès, B., Soulé, J. C., Souquet,
894 P., Ternet, Y. (1984). Carte géologique de la France au 1/50 000, BRGM, Orléans.
895 Feuille d'Arreau n° 1847 avec notice 63 p.

896 Beaumont, C., Muñoz, J. A., Hamilton, J., Fullsack, P. (2000). Factors controlling the Alpine
897 evolution of the central Pyrenees inferred from a comparison of observations and
898 geodynamical models. Journal of Geophysical Research, 105(B4), 8121–8145.
899 https://doi.org/10.1029/1999JB900390

900 Bestani, L., Espurt, N., Lamarche, J., Bellier, O., Hollender, F. (2016). Reconstruction of the
901 Provence Chain evolution, southeastern France. Tectonics, 35.
902 https://doi:10.1002/2016TC004115

903 Beyssac, O., Goffé, B., Chopin, C., Rouzaud, J. N. (2002). Raman spectra of carbonaceous
904 material in metasediments: a new geothermometer. Journal of Metamorphic Geology,
905 20(9), 859–871. http://doi.org/10.1046/j.1525-1314.2002.00408.x

906 Biteau, J.-J., Le Marrec, A., Le Vot, M., Masset, J.-M. (2006). The Aquitaine Basin.
907 Petroleum Geoscience, 12(3), 247–273. https://doi.org/10.1144/1354-079305-674

908 Bourrouilh, R., Richert, J.P., Zolnaie, G. (1995). The North Pyrenean Aquitaine Basin,
909 France: evolution and hydrocarbons. AAPG Bulletin, 79, 831–853.

910 Boutin, A., de Saint Blanquat, M., Poujol, M., Boulvais, P., de Parseval, P., Rouleau, C.,
911 Robert, J.-F. (2016). Succession of Permian and Mesozoic metasomatic events in the

912 eastern Pyrenees with emphasis on the Trimouns talc–chlorite deposit, Int. J. Earth Sci.
913 (Geol Rundsch), 105, 747-770. https://doi.org/ 10.1007/s00531-015-1223-x

914 Boyer, S. E., Elliott, D. (1982). The geometry of thrust systems, AAPG Bulletin, 66, 1196–
915 1230.

916 Bresson, A. E. (1903). Études sur les formations anciennes des Hautes et Basses-Pyrénées
917 (Haute-Chaîne). Vol. 444 de Faculté des Sciences de Paris: Série A, PhD thesis,
918 Béranger, C. (Ed), pp. 278

919 Burg, J. P., Brun, J. P., Van Den Driessche, J. (1990). Le sillon houiller du Massif Central
920 français : faille de transfert pendant l'amincissement crustal de la chaîne. Comptes
921 rendus de l'Académie des sciences. Série 2, Mécanique, Physique, Chimie, Sciences de
922 l'univers, Sciences de la Terre, 311(1), 147-152.

923 Cadenas, P., Fernández-Viejo, G., Pulgar, J. A., Tugend, J., Manatschal, G., Minshull, T. A.
924 (2018). Constraints imposed by rift inheritance on the compressional reactivation of a
925 hyperextended margin: Mapping rift domains in the North Iberian margin and in the
926 Cantabrian Mountains. Tectonics, 37, 758–785. https://doi.org/10.1002/2016TC004454

927 Calderon, Y., Baby, P., Hurtado, C., Brusset, S. (2017). Thrust tectonics in the Andean retro-
928 foreland basin of northern Peru: Permian inheritances and petroleum implications.
929 Marine and Petroleum Geology, 82, 238-250.
930 http://dx.doi.org/10.1016/j.marpetgeo.2017.02.009

931 Calvet, F., Anglada, E., Salvany, J. M. (2004). El Triásico de los Pirineos. In: Vera, J.A. (ed.):
932 Geología de España. SGE-Instituto Geológico y Minero de España, 272–274.

933 Cámara, P., Klimowitz, J. (1985). Interpretación geodinámica de la vertiente Centro-
934 occidental surpirenaica (cuencas de Jaca-Tremp). Estudios Geológicos, 41(5-6), 391–
935 404.

936 Cámara, P., Flinch, J. F. (2017). The Southern Pyrenees: A Salt-Based Fold-and-Thrust Belt.
937 In: Soto, J.I., Flinch, J.F., Tari, G. (Ed.), Permo-Triassic Salt Provinces of Europe,
938 North Africa and the Atlantic Margins., Chapter 18, 395-415, Elsevier Inc.
939 http://dx.doi.org/10.1016/B978-0-12-809417-4.00019-7

940 Canérot, J., Lenoble, J.-L. (1991). Diapirisme sur une marge en distension, puis en
941 décrochement : exemple des Pyrénées occidentales françaises. Excursion et table ronde
942 des 27-28-29 avril 1991. Ed. : Association des sédimentologistes français, Paris, 124 p.

943 Canérot, J., Lenoble, J.-L. (1993). Diapirisme crétacé sur la marge ibérique des Pyrénées
944 occidentales : exemple du pic de Lauriolle ; comparaison avec l'Aquitaine, les Pyrénées
945 centrales et orientales. Bull. Soc. Géol. France, 164(5), 719-726.

946 Canérot, J., Hudec, M. R., Rockenbauch, K. (2005). Mesozoic diapirism in the Pyrenean
947 orogen: Salt tectonics on a transform plate boundary. AAPG Bulletin, 89(2), 211–229.
948 https://doi.org/10.1306/09170404007

949 Carreras, J., Capellà I. (1994). Tectonic levels in the Palaeozoic basement of the Pyrenees: a
950 review and a new interpretation. Journal of Structural Geology, 16(11), 1509-1524.
951 https://doi.org/10.1016/0191-8141(94)90029-9

952 Casas, A., Kearey, P., River, L., Adam, C. R. (1997). Gravity anomaly map of the Pyrenean
953 region and a comparison of the deep geological structure of the western and eastern
954 Pyrenees. Earth and Planetary Science Letters, 150(1-2), 65–78.
955 https://doi.org/10.1016/S0012-821X(97)00087-3

Chevrot, S., Sylvander, M., Diaz, J., Martin, R., Mouthereau, F., Manatschal, G., Masini, E., Calassou, S., Grimaud, F., Pauchet, H., Ruiz, M. (2018). The non-cylindrical crustal architecture of the Pyrenees. Nature Scientific reports, 8, 9591. https://doi.10.1038/s41598-018-27889-x

Chevrot, S., Sylvander, M., Diaz, J., Ruiz, M., Paul, A., and the PYROPE Working Group (2015). The Pyrenean architecture as revealed by teleseismic P-to-S converted waves recorded along two dense transects. Geophysical Journal International, 200, 1096–1107. https://doi:10.1093/gji/ggu400

Choukroune, P., Roure, F., Pinet, B. (1990a). Main results of the ECORS Pyrenees profile. Tectonophysics, 173(1-4), 411–423. https://doi.org/10.1016/0040-1951(90)90234-Y

Choukroune, P., Pinet, B., Roure, F., Cazes M. (1990b). Major Hercynian thrust along the ECORS Pyrenees and Biscay lines. Bulletin de la Société Géologique de France, 2, 313–320. https://doi:10.2113/gssgfbull.VI.2.313

Choukroune, P. (1972). Relations entre tectonique et metamorphisme dans les terrains secondaires de la zone nord-pyrénéenne centrale et orientale. Bulletin de la Société Géologique de France, 7(1-5), 3-11.

Christophoul, F., Soula, J. C., Brusset, S., Elibana, B., Roddaz, M., Bessiere, G., Déramond, J. (2003). Time, place and mode of propagation of foreland basin systems as recorded by the sedimentary fill: Examples of the Late Cretaceous and Eocene retro-foreland basins of the north-eastern Pyrenees. Geological Society, London, Special Publications, 208(1), 229–252. https://doi.org/10.1144/GSL.SP.2003.208.01.11

977 Clerc, C., Lagabrielle, Y. (2014). Thermal control on the modes of crustal thinning leading to
978 mantle exhumation: Insights fom the Cretaceous Pyrenean hot paleomargins. Tectonics,
979 33(7), 1340–1359. https://doi.org/10.1002/2013TC003471

980 Clerc, C., Lagabrielle, Y., Labaume, P., Ringenbach, J. C., Vauchez, A., Nalpas, T., et al
981 (2016). Basement – Cover decoupling and progressive exhumation of metamorphic
982 sediments at hot rifted margin. Insights from the Northeastern Pyrenean analog.
983 Tectonophysics, 686, 82–97. https://doi.org/10.1016/j.tecto.2016.07.022

984 Clerc, C., Ringenbach, J. C., Jolivet, L., Ballard, J. F. (2018). Rifted margins: Ductile
985 deformation, boudinage, continentward-dipping normal faults and the role of the weak
986 lower crust. Gondwana Research, 53, 20-40.

987 Clin M., Taillefer F., Pouchan P., Muller A. (1989). Carte géologique de la France au
988 1/50.000, BRGM, Orléans. Feuille de Bagnères de Luchon n°1986 avec notice 80 p.

989 Cochelin, B., Lemirre, B., Denèle, Y., de Saint Blanquat, M., Lahfid, A., Duchêne, S. (2017).
990 Structural inheritance in the Central Pyrenees: the Variscan to Alpine
991 tectonometamorphic evolution of the Axial Zone. Journal of the Geological Society,
992 16p. https://doi.org/10.1144/jgs2017-066

993 Colletta, B., Roure, F., De Toni, B., Loureiro, D., Passalacqua, H., Gou, Y. (1997). Tectonic
994 inheritance, crustal architecture, and contrasting structural style in the Venezuelan
995 Andes. Tectonics, 16, 777–794. https://doi:10.1029/97TC01659

996 Corre, B., Lagabrielle, Y., Labaume, P., Fourcade, S., Clerc, C., Ballèvre, M. (2016).
997 Deformation associated with mantle exhumation in a distal, hot passive margin
998 environment: New constraints from the Saraillé Massif (Chaînons Béarnais, North-

Pyrenean Zone). Comptes Rendus-Geoscience, 348(3–4), 279–289. https://doi.org/10.1016/j.crte.2015.11.007

Corti, G., Van Wijk, J., Bonini, M., Sokoutis, D., Cloetingh, S., Innocenti, F., Manetti, P. (2003). Transition from continental break-up to punctiform seafloor spreading: How fast, symmetric and magmatic, Geophysical Research Letters, 30(12), 1604. https://doi:10.1029/2003GL017374

Coward, M., Dietrich, D. (1989). Alpine tectonics-an overview. Geological Society, London, Special Publications, 45(1), 1-29.

Crusafont, M., Riba, O., Villena, J. (1966). Nota preliminar sobre un nuevo yacimiento de vertebrados aquitanienses en Sta. Cilia (río Formiga; Provincia de Huesca) y sus consecuencias geológicas. Notas y Com. IGME, 83, pp. 7–13.

Curnelle, R. (1983). Evolution structuro-sédimentaire du Trias et de l'Infra-Lias d'Aquitaine. Bulletin des Centres de Recherches Exploration-Production Elf-Aquitaine, 7(1), 69–99.

Dahlstrom, C. D. A. (1969), Balanced cross sections. Canadian Journal of Earth Sciences, 6(4), 743–757. https://doi.org/10.1139/e69-069

Debroas, E.-J. (1987). Modèle de bassin triangulaire à l'intersection de décrochements divergents pour le fossé albo-cénomanien de la Ballongue. Bulletin de la Société Géologique de France, 8(5), 887–898.

Debroas, E.-J. (1990). Le Flysch noir albo-cénomanien témoin de la structuration albienne à sénonienne de la Zone nord-pyrénéenne en Bigorre (Hautes-Pyrénées, France). Bulletin de La Société Géologique de France, 8(2), 273–285.

1020 Delfaud J. (1966). Le Jurassique et le Néocomien du Mont Sacon (Pyrénées centrales).
1021 Bulletin de La Société Géologique de France, 7, 497-501.

1022 Delfaud J. (1968). Quelques précisions sur le Lias de la région de Rebouc (Hautes-Pyrénées).
1023 Comptes Rendus Sommaires à la Société Géologique de France, 10, 320-321.

1024 Delvolvé, J. J. (1987). Un bassin synorogénique varisque: le Culm des Pyrénées centro-
1025 occidentales. PhD thesis, Université Paul Sabatier Toulouse.

1026 Desegaulx, P., Roure, F., Villien, A. (1990). Structural evolution of the Pyrenees: Tectonic
1027 inheritance and flexural behaviour in the continental crust. Tectonophysics, 182(3–4),
1028 211–225. https://doi.org/10.1016/0040-1951(90)90164-4

1029 De Villechenous F. (1980). Géologie de la partie occidentale du massif varisque de la
1030 Barousse (Pyrénées Centrales). PhD thesis, Université Paul Sabatier Toulouse, 120 p.

1031 Diaz, J., Vergés, J., Chevrot, S., Antonio-Vigil, A., Ruiz, M., Sylvander, M., Gallart, J.
1032 (2018). Mapping the crustal structure beneath the eastern Pyrenees, Tectonophysics,
1033 744, 296-309, https://doi.org/10.1016/j.tecto.2018.07.011

1034 Dreyer, T., Corregidor, J., Arbues, P., Puigdefabregas, C. (1999). Architecture of the
1035 tectonically influenced Sobrarbe deltaic complex in the Ainsa basin, Northern Spain.
1036 Sedimentary Geology 127, 127–169.

1037 Ducoux, M., 2017. Structure, thermicité et évolution géodynamique de la Zone In-terne
1038 Métamorphique des Pyrénées. University of Orléans. https://hal-univ-orleans.archives-
1039 ouvertes.fr/tel-01887025/

1040 Duée, G., Lagabrielle, Y., Coutelle, A., Fortané, A. (1984). Les lherzolites associées aux
1041 Chaînons Béarnais (Pyrénées Occidentales) : Mise à l'affleurement anté-dogger et

1042 resédimentation albo-cénomanienne, Comptes Rendus de l'Académie des Sciences-
1043 Series, 2(299), 1205–1209.

1044 Elliott, D. (1983). The construction of balanced cross sections, Journal of Structural Geology,
1045 5(101). https://doi:10.1016/0191-8141(83)90035-4

1046 Erdős, Z., Huismans, R. S., van der Beek, P., Thieulot, C. (2014). Extensional inheritance and
1047 surface processes as controlling factors of mountain belt structure, J. Geophys. Res.
1048 Solid Earth, 119, 9042–9061, doi:10.1002/ 2014JB011408.

1049 Espurt, N., Brusset, S., Baby, P., Hermoza, W., Bolaños, R., Uyen, D., Déramond, J. (2008).
1050 Paleozoic structural controls on shortening transfer in the Subandean foreland thrust
1051 system, Ene and southern Ucayali basins, Peru. Tectonics, 27, TC3009.
1052 https://doi:10.1029/2007TC002238

1053 Fauré, P. (2002). Le Lias des Pyrénées. PhD thesis, Université Pauk Sabatier-Toulouse III,
1054 Strata, série 2, vol. 39, tome 1; 761 p, 25 pl.

1055 Fernández, O., Muñoz, J.A., Arbués, P. and Falivene, O. (2012). 3D structure and evolution
1056 of an oblique system of relaying folds: The Ainsa basin (Spanish Pyrenees). Journal of
1057 the Geological Society, London, 169, 545–559. http://doi.org/10.1144/0016-76492011-
1058 068

1059 Fitzgerald, P. G., Muñoz, J. A., Coney, P. J., Baldwin, S. L. (1999). Asymmetric exhumation
1060 across the Pyrenean orogen: Implications for the tectonic evolution of a collisional
1061 orogen. Earth and Planetary Science Letters, 173(3), 157–170.
1062 https://doi.org/10.1016/S0012-821X(99)00225-3

1063 Flachère, H. (1977). La nappe du Mont Perdu et ses relations avec la nappe de Gavarnie (Parc
1064 National des Pyrénées occidentales ; Parque Nacional de Ordesa). Thèse 3ème Cycle,
1065 Université Paul Sabatier. Toulouse.

1066 Ford, M., Hemmer, L., Vacherat, A., Gallagher, K., Christophoul, F. (2016). Retro-wedge
1067 foreland basin evolution along the ECORS line, eastern Pyrenees, France. Journal of the
1068 Geological Society, 173(3), 419–437. https://doi.org/10.1144/jgs2015-129

1069 García-Sansegundo, J., Poblet, J., Alonso, J. L., Clariana, P. (2011). Hinterland-foreland
1070 zonation of the Variscan orogen in the Central Pyrenees: comparison with the northern
1071 part of the Iberian Variscan Massif. Geological Society, London, Special Publications,
1072 349(1), 169–184. https://doi.org/10.1144/SP349.9

1073 Garrido-Megías, A. (1973). Estudio geologico y relacion entre tectonica y sedimentacion del
1074 Secundario y Terciario de la vertiente meridional pirenaica en su zona central
1075 (provincias de Huesca y Lerida). Ph.D. thesis. University of Granada, 1-395.

1076 Garrido-Megías, A., Ríos-Aragües, L.M. (1972). Síntesis Geológica del Secundario y
1077 Terciario entre los ríos Cinca y Segre (Pirineo central de la vertiente sur-pirenaica,
1078 provincias de Huesca y Lérida). Boletín Geológico y Minero de España, 83, 1-47.

1079 Gillard, M., Autin, J., Manatschal, G. (2016). Fault systems at hyper-extended rifted margins
1080 and embryonic oceanic crust: Structural style, evolution and relation to magma, Marine
1081 and Petroleum Geology, 76, 51-67, https://doi.org/10.1016/j.marpetgeo.2016.05.013.

1082 Gleizes, G., Leblanc, D., Olivier, P., Bouchez, J. L. (2001). Strain partitioning in a pluton
1083 during emplacement in transpressional regime: the example of the Néouvielle granite
1084 (Pyrenees). International Journal of Earth Sciences 90, 325–340.

1085 Gleizes, G., Crevon, G., Asrat, A., Barbey, P. (2006). Structure, age and mode of
1086 emplacement of the Hercynian Bordères-Louron pluton (Central Pyrenees, France).
1087 International Journal of Earth Sciences, 95(6), 1039–1052.
1088 https://doi.org/10.1007/s00531-006-0088-4

1089 Goldberg, J. M., Leyreloup, A. F. (1990). High temperature-low pressure Cretaceous
1090 metamorphism related to crustal thinning (Eastern North Pyrenean Zone, France).
1091 Contributions to Mineralogy and Petrology, 104, 194–207.

1092 Gong, Z., van Hinsbergen, D.J.J., Vissers, R. L. M., Dekkers, M. J. (2009) Early Cretaceous
1093 syn-rotational extension in the Organyà basin—New constraints on the palinspastic
1094 position of Iberia during its rotation. Tectonophysics,473(3–4), 312-323,
1095 https://doi.org/10.1016/j.tecto.2009.03.003.

1096 Grool, A. R., Ford, M., Vergés, J., Huismans, R. S., Christophoul, F., Dielforder, A. (2018).
1097 Insights into the crustal-scale dynamics of a doubly vergent orogen from a quantitative
1098 analysis of its forelands: A case study of the Eastern Pyrenees. Tectonics, 37, 450–476.
1099 https://doi.org/10.1002/2017TC004731

1100 Harris, N. B. W. (1974). The Petrology and Petrogenesis of Some Muscovite Granite Sills
1101 from the Barousse Massif, Central Pyrenees. Contributions to Mineralogy and
1102 Petrology, 45, 215–230.

1103 Hart, N. R., Stockli, D. F., Lavier, L. L., Hayman, N. W. (2017) Thermal evolution of a
1104 hyperextended rift basin, Mauléon Basin, western Pyrenees, Tectonics, 36, 1103–1128,
1105 doi:10.1002/2016TC004365

1106 Henry, J., Richert, J.-P., Wahbi, Y. (1971). Sur la présence de trois phases tectoniques dans le
1107 Crétacé supérieur de Beyrède-Jumet (Hautes-Pyrénées). Bull. Centre Rech. S.N.P.A.,
1108 Pau, vol. 5, n° 1, 61-87, 10 fig., 2 pl.

1109 Hubschman, J. (1975). Le Plateau de Lannemezan. Bulletin de l'Association Française pour
1110 l'Étude du Quaternaire 12, 207–209.

1111 International Gravimetric Bureau (2012). IAG geodesist's handbook, 2012, Journal of
1112 Geodesy (Vol. 86). Springer.

1113 James, V., Canérot, J. (1999). Diapirisme et structuration post-triasique des Pyrénées
1114 occidentales et de l'Aquitaine méridionale (France). Eclogae geol. Helv., 92, 63-72.

1115 James, V., Canérot, J., Biteau, J.-J. (1996). Données nouvelles sur la phase de rifting
1116 atlantique des Pyrénées occidentales au Kimméridgien : la masse glissée d'Ouzous
1117 (Hautes Pyrénées). Géologie de la France, 3, 60-66.

1118 Jammes, S., Manatschal, G., Lavier, L., Masini, E. (2009). Tectonosedimentary evolution
1119 related to extreme crustal thinning ahead of a propagating ocean: Example of the
1120 western Pyrenees. Tectonics, 28, TC4012. https://doi.org/10.1029/2008TC002406

1121 Jammes, S., Manatschal, G., Lavier, L., 2010a. Interaction between prerift salt and
1122 detachment faulting in hyperextended rift systems: the example of the Parentis and
1123 Mauléon basins (Bay of Biscay andwestern Pyrenees). American Association of
1124 Petroleum Geologists Bulletin, 94 (7), 957–975.

1125 Jammes, S., Tiberi, C., Manatschal, G. (2010b). 3D architecture of a complex transcurrent rift
1126 system: The example of the Bay of Biscay-western Pyrenees. Tectonophysics, 489(1-4),
1127 210–226. https://doi.org/10.1016/j.tecto.2010.04.023

1128 Jammes, S., Huismans, R. S. (2012). Structural styles of mountain building: Controls of
1129 lithospheric rheologic stratification and extensional inheritance. J. Geophys. Res., 117,
1130 B10403, doi:10.1029/2012JB009376

1131 Judge, P. A., Allmendinger, R. W. (2011). Assessing uncertainties in balanced cross sections,
1132 Journal of Structural Geology, 33, 458–467, https://doi:10.1016/j.jsg.2011.01.006

1133 Jolivet, M., Labaume, P., Monié, P., Brunel, M., Arnaud, N., Campani, M. (2007).
1134 Thermochronology constraints for the propagation sequence of the south Pyrenean
1135 basement thrust system (France-Spain). Tectonics, 26(5).

1136 Jourdon, A., Le Pourhiet, L., Mouthereau, F., Masini, E. (2019). Role of rift maturity on the
1137 architecture and shortening distribution in mountain belts. Earth and Planetary Science
1138 Letters, 512, 89–99.

1139 Jourdon, A., Rolland, Y., Petit, C., Bellahsen, N. (2014). Style of Alpine tectonic deformation
1140 in the Castellane fold-and-thrust belt (SW Alps, France): Insights from balanced cross-
1141 sections. Tectonophysics, 633, 143-155. http://dx.doi.org/10.1016/j.tecto.2014.06.022

1142 Labaume, P., Meresse, F., Jolivet, M., and Teixell, A. (2016a). Exhumation sequence of the
1143 basement thrust units in the west-central Pyrenees. Constraints from apatite fission track
1144 analysis. Geogaceta, 60, 11-14.

1145 Labaume, P., Meresse, F., Jolivet, M., Teixell, A., Lahfid, A. (2016b). Tectonothermal history
1146 of an exhumed thrust-sheet-top basin: An example from the south Pyrenean thrust belt.
1147 Tectonics, 35(5), 1280–1313. https://doi.org/10.1002/2016TC004192

1148 Lacombe, O., Bellahsen, N. (2016). Thick-skinned tectonics and basement-involved fold–
1149 thrust belts: insights from selected Cenozoic orogens. Geological Magazine, 153(5/6),
1150 763–810. doi:10.1017/S0016756816000078

1151 Lagabrielle, Y., Labaume, P., Clerc, C., de Saint Blanquat, M., Lahfid, A., et al. (2016).
1152 Diversité des conditions thermiques lors de l'exhumation du manteau de la Zone Nord-
1153 Pyrénéenne : bilan des contraintes géologiques. 25ème Réunion des sciences de la Terre
1154 (RST 2016), Oct 2016, Caen, France. Livre des résumés, p. 182.

1155 Lagabrielle, Y., Labaume, P., de Saint Blanquat, M. (2010), Mantle exhumation, crustal
1156 denudation, and gravity tectonics during Cretaceous rifting in the Pyrenean realm (SW
1157 Europe): Insights from the geological setting of the lherzolite bodies. Tectonics, 29,
1158 TC4012. https://doi:10.1029/2009TC002588

1159 Lagabrielle, Y., Bodinier, J. L. (2008). Submarine reworking of exhumed subcontinental
1160 mantle rocks: Field evidence from the Lherz peridotites, French Pyrenees. Terra Nova,
1161 20(1), 11–21. https://doi:10.1111/j.1365-3121.2007.00781.x

1162 Lahfid, A., Beyssac, O., Deville, E., Negro, F., Chopin, C., Goffé, B. (2010). Evolution of the
1163 Raman spectrum of carbonaceous material in low-grade metasediments of the Glarus
1164 Alps (Switzerland). Terra Nova, 22(5), 354–360. https://doi.org/10.1111/j.1365-
1165 3121.2010.00956.x

1166 Le Roux, V., Bodinier, J.-L., Tommasi, A., Alard, O., Dautria, J.-M., Vauchez, A., Riches,
1167 A.J.V. (2007). The Lherz spinel lherzolite: Refertilized rather than pristine mantle,
1168 Earth and Planetary Science Letters- 259, 599-612. https://doi.org/
1169 10.1016/j.epsl.2007.05.026

1170 Le Vot, M., Biteau, J. J., Masset, J. M. (1996). The Aquitaine basin: Oil and gas production in
1171 the foreland of the Pyrenean fold-and-thrust belt, new exploration perspectives. In P. A.
1172 Ziegler and F. Horvath (Eds), Peri-Tethys memoir 2: Structure and prospects of Alpine
1173 basins and forelands: Mémoires du Museum National d'Histoire Naturelle, 170, 159–
1174 171.

1175 López-Mir, B., Anton Muñoz, J., García Senz, J. (2014a). Extensional salt tectonics in the
1176 partially inverted Cotiella post-rift basin (south-central Pyrenees): structure and
1177 evolution. Int J Earth Sci (Geol Rundsch), https://doi.org/10.1007/s00531-014-1091-9

1178 López-Mir, B., Anton Muñoz, J., García Senz, J. (2014b). Restoration of basins driven by
1179 extension and salt tectonics: Example from the Cotiella Basin in the central Pyrenees.
1180 Journal of Structural Geology, 69, 147–162. https://doi.org/10.1016/j.jsg.2014.09.022

1181 Lucas, C. (1985). Le grès rouge du versant nord des Pyrénées: essai sur la géodynamique de
1182 dépôts continentaux du Permien et du Trias. Thèse de Doctorat, Université de Toulouse
1183 III – Paul Sabatier, Toulouse, 268 p.

1184 Lucas, C. (1968). Le « grès rouge » du Comminges et de la Bigorre (Pyrénées Centrales).
1185 Etude géologique. Thèse 3ème cycle, Toulouse, 131 p, 12 planches.

1186 Macchiavelli, C., Vergés, J., Schettino, A., Fernàndez, M., Turco, E., Casciello, E., et al
1187 (2017). A new southern North Atlantic isochron map: Insights into the drift of the
1188 Iberian plate since the Late Cretaceous. Journal of Geophysical Research: Solid Earth,
1189 122, 9603–9626. https://doi.org/10.1002/2017JB014769

1190 Manatschal, G., Lavier, L., Chenin, P. (2015). The role of inheritance in structuring
1191 hyperextended rift systems: Some considerations based on observations and numerical
1192 modeling. Gondwana Research, 27, 140-164, https://doi.org/10.1016/j.gr.2014.08.006

1193 Martinez-Peña, B., Casas-Sainz, A. M. (2003). Cretaceous-Tertiary tectonic inversion of the
1194 Cotiella Basin (southern Pyrenees, Spain). International Journal of Earth Sciences,
1195 92(1), 99–113. https://doi.org/10.1007/s00531-002-0283-x

1196 Martínez Peña, B., Pocoví, A. (1998). El amortiguamiento frontal de la estructura de la
1197 cobertera Surpirenaica y su relación con el anticlinal de Barbastro–Balaguer. Acta Geol.
1198 Hisp. 23, 81–94.

1199 Masini, E., Manatschal, G., Tugend, J., Mohn, G., Flament, J. M. (2014), The tectono-
1200 sedimentary evolution of a hyper-extended rift basin: The example of the Arzacq–
1201 Mauléon rift system (Western Pyrenees, SW France), Int. J. Earth Sci., 1–28,
1202 https://doi.org/10.1007/s00531-014-1023-8

1203 Mattauer, M. (1990). Une autre interprétation du profil ECORS Pyrénées. Bulletin de la
1204 Societé Géologique de France, 6(2), 307-311.

1205 McClay, K., Muñoz, J.A., García-Senz, J. (2004). Extensional salt tectonics in a contractional
1206 orogen: a newly identified tectonic event in the Spanish Pyrenees. Geology 32(9), 737-
1207 740.

1208 Mirouse, R., Barrère, P., Souquet, P., Flachere, H., Joseph, J., Lamouroux, C., et al (1993).
1209 Carte géologique de la France au 1/50000, BRGM, Orléans. Feuille de Vieille-Aure
1210 n°1083 avec notice 107 p.

1211 Mitra, S., Namson, J. (1989). Equal-area balancing. American Journal of Science, 289, 563-
1212 599.

1213 Montigny, R., Azambre, B., Rossy, M., Thuizat, R. (1986). K-Ar study of Cretaceous
1214 magmatism and metamorphism in the Pyrenees: age and length of rotation of the Iberian
1215 Peninsula. Tectonophysics, 129, 257-273.

1216 Mouchené, M., van der Beek, P., Mouthereau, F., Carcaillet, J. (2017). Controls on
1217 Quaternary incision of the Northern Pyrenean foreland: Chronological and
1218 geomorphological constraints from the Lannemezan megafan, SW France.
1219 Geomorphology, 281, 78–93. http://dx.doi.org/10.1016/j.geomorph.2016.12.027

1220 Mouchené, M. (2016). Évolution post-orogénique du système couplé piémont / bassin
1221 versant : le méga-cône alluvial de Lannemezan et son bassin versant au Nord des
1222 Pyrénées. PhD Thesis Univ. de Grenoble. Université Grenoble Alpes.

1223 Mouthereau, F., Filleaudeau, P., Vacherat, A., Pik, R., Lacombe, O., Fellin,M. G.,…Masini,
1224 E. (2014). Placing limits to shortening evolution in the Pyrenees: Role of margin
1225 architecture and implications for the Iberia/Europe convergence. Tectonics, 33, 2283–
1226 2314. https://doi.org/10.1002/2014TC003663

1227 Mochales, T., Casas, A. M., Pueyo, E. L., Barnolas, A. (2012). Rotational velocity for oblique
1228 structures (Boltaña anticline, Southern Pyrenees), Journal of Structural Geology, 35, 2–
1229 16. https://doi:10.1016/j.jsg.2011.11.009

1230 Morris, R. G., Sinclair, H. D., Yell, A. J. (1998). Exhumation of the Pyrenean orogen:
1231 implications for sediment discharge. Basin Research, 10, 69–85.
1232 https://doi:10.1046/j.1365-2117.1998.00053.x

1233 Muñoz, J. A., Beamud, E., Fernández, O., Arbués, P., Dinarès-Turell, J., Poblet, J. (2013).
1234 The Ainsa Fold and Thrust Oblique Zone of the central Pyrenees: kinematics of a

curved contractional system from paleomagnetic and structural data. Tectonics 32(5), 1142–1175.

Muñoz, J. A. (1992). Evolution of a continental collision belt: ECORS-Pyrenees crustal balanced cross-section. In Thrust Tectonics, Mc Clay, K. (Ed), 235–246, Chapman and Hall, London.

Muñoz, J. A., Martínez, A., Vergés, J. (1986). Thrust sequences in the eastern Spanish Pyrenees. Journal of Structural Geology, 8, 399-405.

Mutti, E., Remacha, E., Sgavetti, M., Rosell, J., Valloni, R., Zamorano, M. (1985). Stratigraphy and facies characteristics of the Eocene Hecho Group turbidite systems, south-central Pyrenees. Excursion 12, in 6th European Regional Meeting Excursion Guidebook - IAS, edited by M. D. Milà and J. Rosell, pp. 519–576, Inst. Estud. Ilerdencs, Lleida, Spain.

Olivet, J. (1996). La cinématique de la plaque ibérique. Bulletin des Centres de Recherches Exploration-Production Elf-Aquitaine, 20(1), 131–195.

Paris, J. P., Icole, M. (1975). Carte géologique de la France au 1/50 000, BRGM, Orléans. Feuille de Montréjeau n° 1054 avec notice 25 p.

Poblet, J., Muñoz, J. A., Travé, A., Serra-Kiel, J. (1998). Quantifying the kinematics of detachment folds using three-dimensional geometry: Application to the Mediano anticline (Pyrenees, Spain), Geol. Soc. Am. Bull., 110(1), 111–125.

Puigdefàbregas, C. (1975). La sedimentación molásica en la cuenca de Jaca. Monogr. del Inst. Estud. Piren. 104, 1-188.

1256 Puigdefàbregas, C., Souquet, P. (1986). Tecto-sedimentary cycles and depositional sequences
1257 of the Mesozoic and Tertiary from the Pyrenees. Tectonophysics 129, 173-203.
1258 doi:10.1016/0040-1951(86)90251-9

1259 Quirantes Puertas, J. (1969). Estudio sedimentologico y estratigrafico del terciaro continental
1260 de los Monegros (Doctoral dissertation, Tesis (CSIC), Zaragoza).

1261 Rat, J., Mouthereau, F., Brichau, S., Crémades, A., Bernet, M., Balvay, M., et al. (2019).
1262 Tectonothermal evolution of the Cameros basin: Implications for tectonics of North
1263 Iberia. Tectonics, 38, 440–469. https://doi.org/10.1029/2018TC005294

1264 Ravier, J. (1957). Le métamorphisme des terrains secondaires des Pyrénées. Thèse 3e cycle,
1265 Université de Toulouse.

1266 Riba, O., Reguant, S., Villena, J. (1983). Ensayo de sintesis estratigrafica y evolutiva de la
1267 cuenca terciaria del Ebro. Libro Jubilar J.M. Rios. Geologia de Espana, v. II, 131-159

1268 Roca, E., Muñoz, J. A., Ferrer, O., Ellouz, N. (2011). The role of the Bay of Biscay Mesozoic
1269 extensional structure in the configuration of the Pyrenean orogen: constraints from the
1270 MARCONI deep seismic reflection survey. Tectonics 30, TC2001.
1271 https://doi.org/10.1029/2010TC002735

1272 Rocher, M., Lacombe, O., Angelier, J., Deffontaines, B., Verdier, F. (2000). Cenozoic folding
1273 and faulting in the south Aquitaine Basin (France): insights from combined structural
1274 and paleostress analyses. Journal of Structural Geology, 22, 627-645.

1275 Roddaz, B. (1977). Le prolongement oriental de la nappe de Gavarnie et son substratum entre
1276 Barroude et le Moudang (Pyrénées centrales). Thèse 3e cycle, Université de Toulouse,
1277 131 p., 79 fig.

1278 Román-Berdiel, T., Casas, A. M., Oliva-Urcia, B., Pueyo, E. L., Rillo, C. (2004). The main
1279 Variscan deformation event in the Pyrenees: new data from the structural study of the
1280 Bielsa granite. Journal of Structural Geology, 26(4), 659-677.

1281 Rougier, G., Ford, M., Christophoul, F., Bader, A.-G. (2016). Stratigraphic and tectonic
1282 studies in the central Aquitaine Basin, northern Pyrenees: Constraints on the subsidence
1283 and deformation history of a retro-foreland basin. Comptes Rendus Geoscience, 348(3–
1284 4), 224–235. https://doi.org/10.1016/j.crte.2015.12.005

1285 Roure, F., Colletta, B. (1996). Cenozoic inversion structures in the foreland of the Pyrenees
1286 and Alps. In: Ziegler, P., Horvath, F. (Eds.), PeriTethys Memoir, 2. Museum d'Histoire
1287 Naturelle, Paris, 173–210.

1288 Roure, F., Choukroune, P., Berastegui, X., Muñoz, J. A., Villien, A., Matheron, P.,
1289 Déramond, J. (1989). Ecors deep seismic data and balanced cross sections: Geometric
1290 constraints on the evolution of the Pyrenees. Tectonics, 8(1), 41–50.
1291 https://doi.org/10.1029/TC008i001p00041

1292 Santolaria, P., Casas-Sainz, A. M., Soto, R., Pinto, V., Casas, A. (2014). The Naval diapir
1293 (southern Pyrenees): Geometry of a salt wall associated with thrusting at an oblique
1294 ramp. Tectonophysics, 637, 30–44. https://doi.org/10.1016/j.tecto.2014.09.008

1295 Santolaria, P., Casas-Sainz, A. M., Soto, R., Casas, A. (2016). Gravity modelling to assess
1296 salt tectonics in the western end of the South Pyrenean Central Unit. Journal of the
1297 Geological Society, 174, 269-288. https://doi.org/10.1144/jgs2016-027

1298 Saspiturry, N., Cochelin, B., Razin, P., Leleu, S., Lemirre, B., Issautier, B., Serrano, O.,
1299 Lasseur, E., Baudin, T. (2018). Post-Hercynian tectono-sedimentary evolution of an
1300 extensive intra-continental rift basin controlled by the upwelling of a metamorphic core

complex (Bidarray Basin, Western Pyrenees). 26ème Réunion des sciences de la Terre (RST 2018), Oct 2018, Lille, France. Livre des résumés, p. 177.

Saura, E., Teixell, A. (2006). Inversion of small basins: effects on structural variations at the leading edge of the Axial Zone antiformal stack (Southern Pyrenees, Spain). Journal of Structural Geology, 28, 1909-1920.

Séguret, M. (1972), Etude tectonique des nappes et séries décollées de la partie centrale du versant sud des Pyrénées, Sér. Géol. Struct. n° 2, USTELA, Montpellier, France.

Serrano, O. (2015). Histoire de l'exploration des hydrocarbures du bassin d'Aquitaine. Géosciences, 19, 32-41, BRGM (Ed), Orléans.

Serrano, O., Delmas, J., Hanot, F., Vially, R., Herbin, J.-P., Houel, P., Tourlière, B. (2006). Le bassin d'Aquitaine : valorisation des données sismiques, cartographique structurale et potentiel pétrolier, BRGM (Ed), Orléans.

Sibuet, J.-C., Srivastava, S. P., Spakman, W. (2004). Pyrenean orogeny and plate kinematics. Journal of Geophysical Research, 109, B08104, https://doi:10.1029/2003JB002514

Simancas, J.F., Martinez Poyatos, D., Exposito, I., Azor, A., Gonzalez Lodeiro, F. (2001). The structure of a major suture zone in the SW Iberian Massif: the Ossa-Morena/Central Iberian contact, Tectonophysics, 332, 295–308.

Simancas, J.F. et al., (2003). Crustal structure of the transpressional Variscan orogen of SW Iberia: SW Iberia deep seismic reflection profile (IBERSEIS), Tectonics, 22(6), 1062, doi:10.1029/2002TC001479

1321 Soler, D., Teixell, A., Garcia-Sansegundo, J. (1998). Amortissement latéral du
1322 chevauchement de Gavarnie et sa relation avec les unités sud-pyrénéennes, Comptes
1323 Rendus de l'Académie des Sciences, Earth and Planetary Science, 327, 699–704.

1324 Soto, R., Casas, A. M., Storti, F., Faccenna, C. (2002). Role of lateral thickness variation on
1325 the development of oblique structures at the western end of the south Pyrenean central
1326 unit. Tectonophysics, 350, 215–235.

1327 Soula, J.-C. (1982). Characteristics and mode of emplacement of gneiss domes and plutonic
1328 domes in central-eastern Pyrenees. Journal Structural Geology, 4, 313–342.
1329 https://doi:10.1016/0191-8141(82)90017-7

1330 Soula, J.-C., Debat, P. Déramond, J., Pouget, P. (1986). A dynamic model of the structural
1331 evolution of the Hercynian Pyrenees, Tectonophysics, 129, 29-51,
1332 https://doi.org/10.1016/0040-1951(86)90244-1

1333 Souquet, P., Delvolvé, J.-J., Brusset, S. (2003). Identification of an underfilled foreland basin
1334 system in the Upper Devonian of the Central Pyrenees: implications for the Hercynian
1335 orogeny. International Journal of Earth Sciences, 92(3), 316–337.
1336 https://doi.org/10.1007/s00531-003-0334-y

1337 Souquet, P., Debroas, E.-J., Boirie, J.-M., Pons, P., Fixari, G., Roux, J.-C., et al (1985). Le
1338 groupe du flysch noir (Albo-Cénomanien) dans les Pyrénées. Bulletin Des Centres de
1339 Recherche Exploration-Production Elf-Aquitaine, 9(1), 183–252.

1340 Souquet, P., Peybernes, B., Bilotte, M., Debroas, E. J. (1977). La chaîne Alpine des Pyrénées.
1341 Géologie Alpine, 53, 193-216.

1342 Tavani, S., Bertok, C., Granado, P., Piana, F., Salas, R., Vigna, B., Muñoz, J.A., (2018). The
1343 Iberia-Eurasia plate boundary east of the Pyrenees, Earth-Science Reviews,
1344 https://doi.org/10.1016/j.earscirev.2018.10.008.

1345 Teixell, A., Labaume, P., Ayarza, P., Espurt, N., de Saint Blanquat, M., Lagabrielle, Y.
1346 (2018). Crustal structure and evolution of the Pyrenean-Cantabrian belt: A review and
1347 new interpretations from recent concepts and data. Tectonophysics, 724–725, 146-170,
1348 https://doi.org/10.1016/j.tecto.2018.01.009

1349 Teixell, A., Labaume, P., Lagabrielle, Y. (2016). The crustal evolution of the west-central
1350 Pyrenees revisited: Inferences from a new kinematic scenario. Comptes Rendus
1351 Geoscience, 348(3-4), 257–267. https://doi.org/10.1016/j.crte.2015.10.010

1352 Teixell, A., Durney, D. W., Arboleya, M. L. (2000). Stress and fluid control on décollement
1353 within competent limestone. Journal of structural geology, 22(3), 349–371.
1354 https://doi.org/10.1016/S0191-8141(99)00159-5

1355 Teixell, A. (1998). Crustal structure and orogenic material budget in the west central
1356 Pyrenees. Tectonics, 17(3), 395–406. https://doi.org/10.1029/98TC00561

1357 Teixell, A. (1996). The Ansó transect of the southern Pyrenees: Basement and cover thrust
1358 geometries. Journal of geological society, 153, 301–310.

1359 Teixell, A., Barnolas, A. (1995). Significado de la discordancia de Mediano en relación con
1360 las estructuras adyacentes (Pirine central). Geogaceta 17, 186–189.

1361 Ternet, Y., Barrère, P. Debroas, E. J. (1995). Carte géologique de la France au 1/50 000,
1362 BRGM, Orléans. Feuille de Campan n°1071 avec notice 117 p.

1363 Tugend, J., Manatschal, G., Kusznir, N. J. (2015). Spatial and temporal evolution of
1364 hyperextended rift systems: Implication for the nature, kinematics, and timing of the
1365 Iberian-European plate boundary. Geology, 43(1), 15–18.
1366 https://doi.org/10.1130/G36072.1

1367 Vacherat, A., Mouthereau, F., Pik, R., Huyghe, D., Paquette, J.-L., Christophoul, F., et al
1368 (2017). Rift-to-collision sediment routing in the Pyrenees: A synthesis from
1369 sedimentological, geochronological and kinematic constraints. Earth-Science Reviews,
1370 172, 43–74. https://doi.org/10.1016/j.earscirev.2017.07.004

1371 Vacherat, A., Mouthereau, F., Pik, R., Bernet, M., Gautheron, C., Masini, E., Le Pourhiet, L.,
1372 Tibari, B., Lahfid, A. (2014), Thermal imprint of rift related processes in orogens as
1373 recorded in the Pyrenees, Earth Planetary Science Letters, 408, 296–306.

1374 Velasque, P. C., Ducasse, L., Muller, J., Scholten, R. (1989). The influence of inherited
1375 extensional structures on the tectonic evolution of an intracratonic chain: the example of
1376 the Western Pyrenees. Tectonophysics, 162, 243–264.

1377 Vergés, J., Ramos, V. A., Meigs, A., Cristallini, E., Bettini, F. H., Cortés, J. M. (2007).
1378 Crustal wedging triggering recent deformation in the Andean thrust front between 31°S
1379 and 33°S: Sierras Pampeanas-Precordillera interaction, Journal of Geophysical
1380 Research, 112,B03S15. https://doi:10.1029/2006JB004287

1381 Vergés, J., García-Senz, J. (2001). Mesozoic evolution and Cainozoic inversion of the
1382 Pyrenean Rift, in Peri-Tethys Memoir 6: Peri-Tethyan Rift/Wrench Basins and Passive
1383 Margins, Mém. Mus. Natl. Hist. Nat., vol. 186, edited by P. A. Ziegler et al., pp. 187–
1384 212, Paris.

1385 Vergés, J., Millan, H., Roca, E., Muñoz, J. A., Marzo, M., Cirés, J., et al (1995). Eastern
1386 Pyrenees and related foreland basins: Pre-, syn- and post-collisional crustal-scale cross-
1387 sections. Marine and Petroleum Geology, 12(8), 893–915.

1388 Vergés, J., Muñoz, J.A., Martínez, A. (1992). South Pyrenean fold and thrust belt: The role of
1389 foreland evaporitic levels in thrust geometry. McClay, K. Thrust Tectonics. Chapman
1390 Hall, London, 255-264.

1391 Vielzeuf, A., Kornprobst, J. (1984). Crustal splitting and the emplacement of Pyrenean
1392 lherzolites and granulites. Earth Planetary Science Letters, 67, 87-96.

1393 Vissers, R.L.M., Drury, M.R., Newman, J., Fliervoet, T.F. (1997). Mylonitic deformation in
1394 upper mantle peridotites of the North Pyrenean Zone (France): implications for strength
1395 and strain localization in the lithosphere, Tectonophysics, 279, 303-325,
1396 https://doi.org/10.1016/S0040-1951(97)00128-5.

1397 Vissers, R.L.M. (1992). Variscan extension in the Pyrenees. Tectonics, 11, 1369-1384.

1398 Specht, M. (1989). Tectonique de chevauchement le long du profil ECORS-Pyrénées: un
1399 modèle d'évolution de prisme d'accrétion continental, PhD thesis, 99, 353 pp., Univ. de
1400 Bretagne Occident. de Brest (Sci.).

1401 Wallace, W. K. (2008). Yakataga fold-and-thrust belt: Structural geometry and tectonic
1402 implications of a small continental collision zone, in Active Tectonics and Seismic
1403 Potential of Alaska, edited by J. T. Freymueller et al., pp. 237–256, AGU, Washington,
1404 D. C., https://doi:10.1029/179GM13

Wang, Y., Chevrot, S., Monteiller, V., Komatitsch, D., Mouthereau, F., Manatschal, G., et al (2016). The deep roots of the western Pyrenees revealed by full waveform inversion of teleseismic P waves. Geology, 44(6), 475–478.

Fig.1: Geological setting of the Pyrenean orogen. NPFT: North Pyrenean Frontal Thrust. NPZ: North Pyrenean Zone. NPFZ: North Pyrenean Fault Zone. SPZ: South Pyrenean Zone. SPFT: South Pyrenean Frontal Thrust. Co: Cotiella. Cl: Clamosa. Na: Naval. ECL: Eastern Crustal Lineament. Lzn: Lannemezan. St-Gds: Saint-Gaudens. The thick white line shows location of the Nestes-Cinca balanced cross section of this study. The section follows the trace of the LR06 seismic profile (dashed white line) and the OROGEN West profile (black line). White circles indicate exploration wells.

Fig. 2: Stratigraphic and lithotectonic sedimentary sections in the different tectonic units in the Central Pyrenees along the Nestes-Cinca transect. A synthetic stratigraphic column from exploration wells is shown for the Aquitaine Basin. Black and white half arrows: extensional faults. Red and white half arrows: Pyrenean thrusts.

Fig. 3: Geological maps of the North Pyrenean Zone and Axial Zone. For location, see Fig. 1. The white line shows trace of the Nestes-Cinca cross section. The southern edge of the seismic reflection profile LR06 is shown. Peak paleo-temperature values (°C) deduced by Raman spectroscopy of carbonaceous material are indicated by red diamonds and numbers (see Table 1). Pa: Pariou. HV: Houle Verte. U: Urgonian facies.

Fig. 4: Geological field observations in the North Pyrenean Zone along the Nestes valley. For location, see Fig. 3. (a) Upper Jurassic dolomitic breccias of the Léchan thrust (Hèches quarry). (b) Albian Black flysch strata near Izaux town. (c) Tectonic slices of lherzolite, Triassic shales and Urgonian limestones in the Avezac thrust (Avezac town quarry). (d) Foliation and boudinage within overturned middle-upper Albian limestones (east of Esparros town, col de Coupe). (e) Mylonite of Albian-Cenomanian? sedimentary breccias including Jurassic and Cretaceous carbonate, ophitic, red beds and Ordovician clasts (Houle Verte marble quarry). (f) Pre-folding bedding-parallel boudinage (S0-S1) in Cenomanian breccias in the Beyrède syncline including Triassic and fractured Jurassic clasts (Beyrède marble quarry). (g) and (h): Pre-folding bedding-parallel fabric (S0-S1) and polyphase ductile deformations (S2, S3) in Albian Black flysch (Baronnies zone) and Cenomanian limestones (Beyrède syncline, Montillet zone), respectively. Carbonate rocks in (c), (e) and (f) have been sampled for Raman Spectroscopy of Carbonaceous Material (see Table 1).

Fig. 5: Structural interpretation of the depth-converted seismic profile LR06 across the southern edge of the Aquitaine Basin and northern edge of the North Pyrenean Zone (NPZ) calibrated with eleven exploration wells (see Supplementary material Fig. S1 for well details and Table S1 for data of time-depth conversion). For location, see Fig. 1. We interpret the deep tectonic slice under the North Pyrenean Zone as the western continuation of the Saint-Gaudens dense body (SGDB). NPFT: North Pyrenean Frontal Thrust.

Fig. 6: Surficial cross-sectional geometry of (a) the southern part of the North Pyrenean Zone-Axial Zone and (b) South Pyrenean Zone-northern edge of the Ebro Basin in the Central Pyrenees along the Nestes-Cinca transect. The surface geometry of the South Pyrenean Zone is modified from López-Mir et al. (2014), Teixell and Barnolas (1995), Cámara and Flinch (2017) and Santolaria et al. (2016). For locations, see Figs. 1 and 3. Dashed thin red lines indicate foliations. NPFZ: North Pyrenean Fault Zone. SG: Sarrancolin granite. BLG: Bordères-Louron granite.

Fig. 7: Details of the North Pyrenean Zone structure and peak paleo-temperatures (°C) deduced from Raman spectroscopy. The data have been projected onto the section (red numbers and diamonds; see Fig. 3 and Table 1). For legend, see Fig. 6.

Fig. 8: Panoramic views in the North Pyrenean Zone along the Neste River. (a) Lortet and Estivère anticlines in the northern external metamorphic zone. (b) Southern border of the northern external metamorphic zone. (c) Southern internal metamorphic zone (Montillet zone) and North Pyrenean Fault Zone. (d) Panoramic view looking westward of the Aure trough filled by Permian-Triassic red beds (Arreau unit). For locations, see Figs. 3, 6a and 7. Syncline cores are indicated by U-shape.

Fig. 9: Pyrenean faults in the northern part of the Axial Zone. (a) The Beyrède thrust bounding the North Pyrenean Zone and the Axial Zone. (b) The Arreau thrust near Jézeau town. For location, see Figs. 3, 6a and 7.

Fig. 10: Panoramic views in the Axial Zone. (a) and (b): Variscan thrust systems in the Vielle-Aure Basin (Gavarnie thrust sheet). (c): South-verging Pyrenean Gavarnie thrust overthrusting the Bielsa unit in the Neste de Saux valley. For location, see Figs. 3 and 6a.

Fig. 11: Stack profile of receiver functions for the OROGEN West profile across the Central Pyrenean belt. See data acquisition and method in Chevrot et al. (2018). The interpretation is modified from Teixell et al. (2018) and Chevrot et al. (2018). For location, see Fig. 1. The gravity anomaly profile along the section is also shown (data from the International Gravimetric Bureau, 2012). For labels and legend, see Figs. 6 and 12.

Fig. 12: (a) Present-day crustal-scale balanced cross section of the Central Pyrenees along the Nestes-Cinca transect. (b) Lower Santonian restoration of the Cretaceous Pyrenean Rift system. For location, see Fig. 1. See details of the restored Pyrenean Rift system in Fig. 13. NPFT: North Pyrenean Frontal Thrust. NPFZ: North Pyrenean Fault Zone. SPFT: South Pyrenean Frontal Thrust. SGDB: Saint-Gaudens dense body. Black and white half arrows: extensional faults. Red and white half arrows: Pyrenean thrusts.

Fig. 13: Details of the restored Cretaceous Pyrenean Rift system during the early Santonian. Labels as in Fig. 12. Peak paleo-temperatures (°C) deduced from Raman spectroscopy of carbonaceous material are indicated by red numbers (see Table 1 and Fig. 3). White dashed line indicates approximately the 450°C isotherm.

Fig. 14: Inferred sequential restoration of the pre-orogenic evolution of the Central Pyrenean domain. (a) Lower Santonian restoration showing the structural architecture of the Cretaceous Pyrenean Rift system. (b) Structural architecture of the middle Triassic-Jurassic extensional system. (c) Restoration of the Variscan thrust belt and post-Variscan Permian extensional structures sealed by lower-middle Triassic red beds. Labels as in Fig. 12. Black half arrows: Variscan thrusts. Black and white half arrows: extensional faults or inferred strike-slip movements.

Fig. S1: Exploration wells across the Aquitaine Basin used to calibrate the LR06 seismic profiles. For more details, see http://infoterre.brgm.fr/.

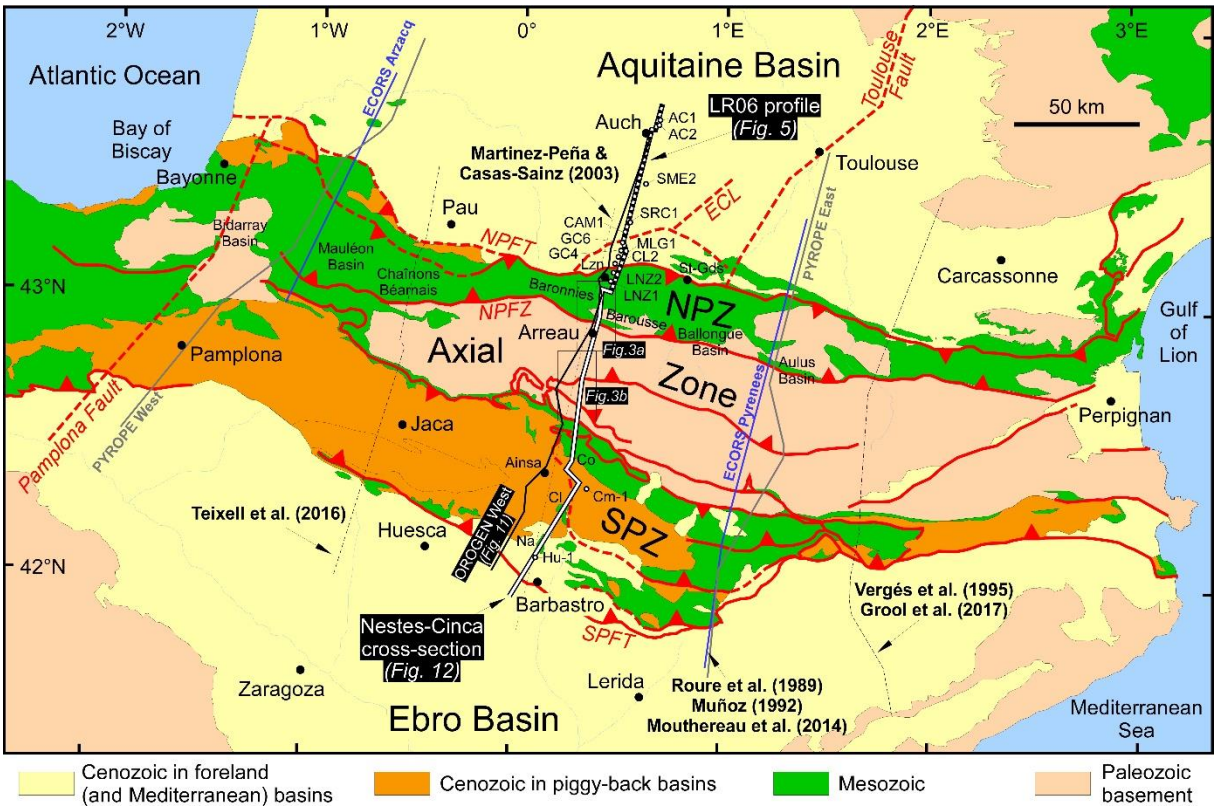

1491

1492 Figure 1

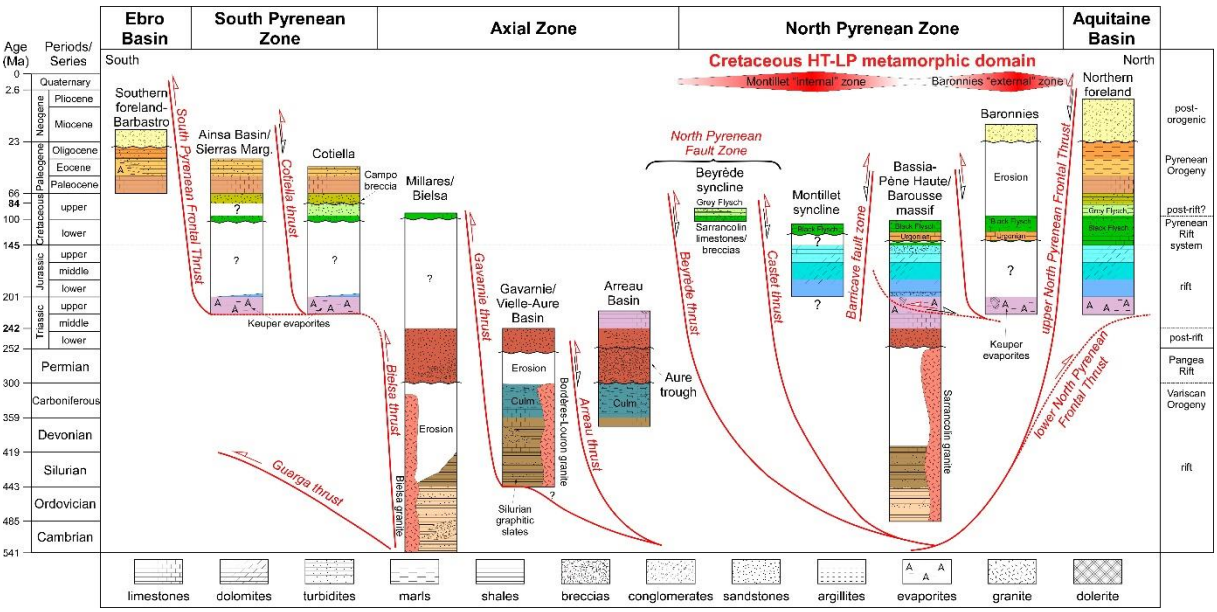

1493

1494 Figure 2

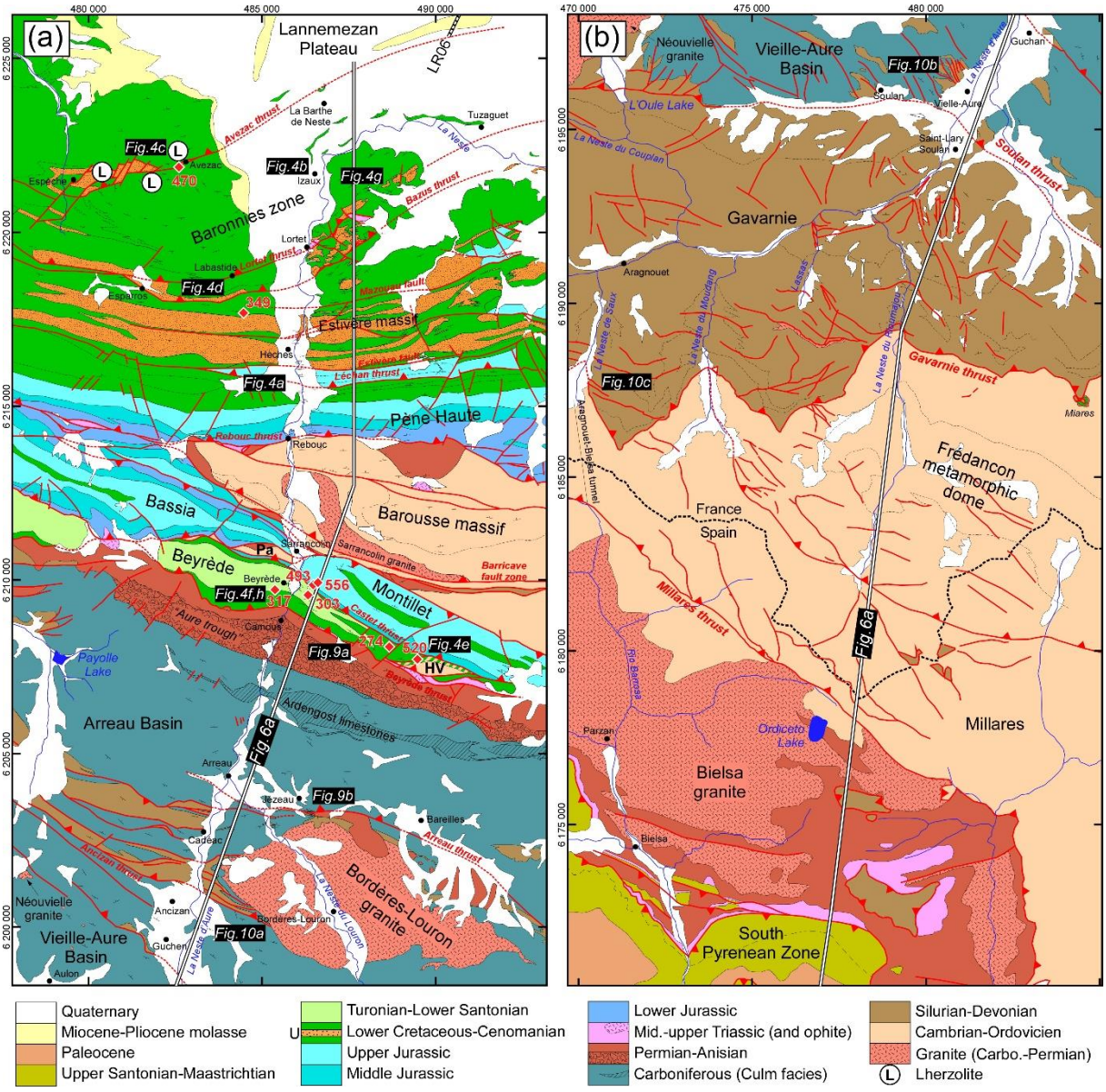

1495

1496 Figure 3

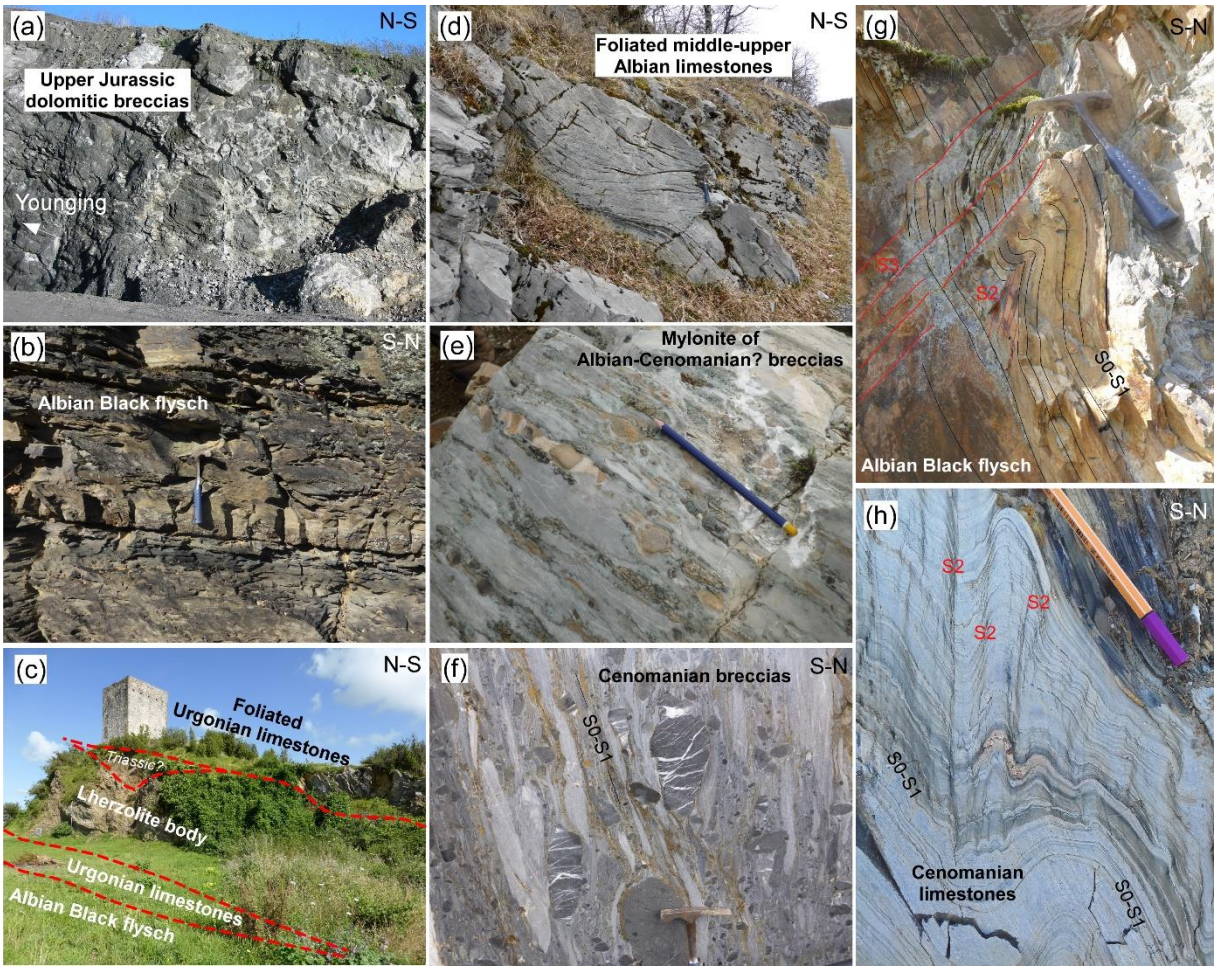

1497

1498 Figure 4

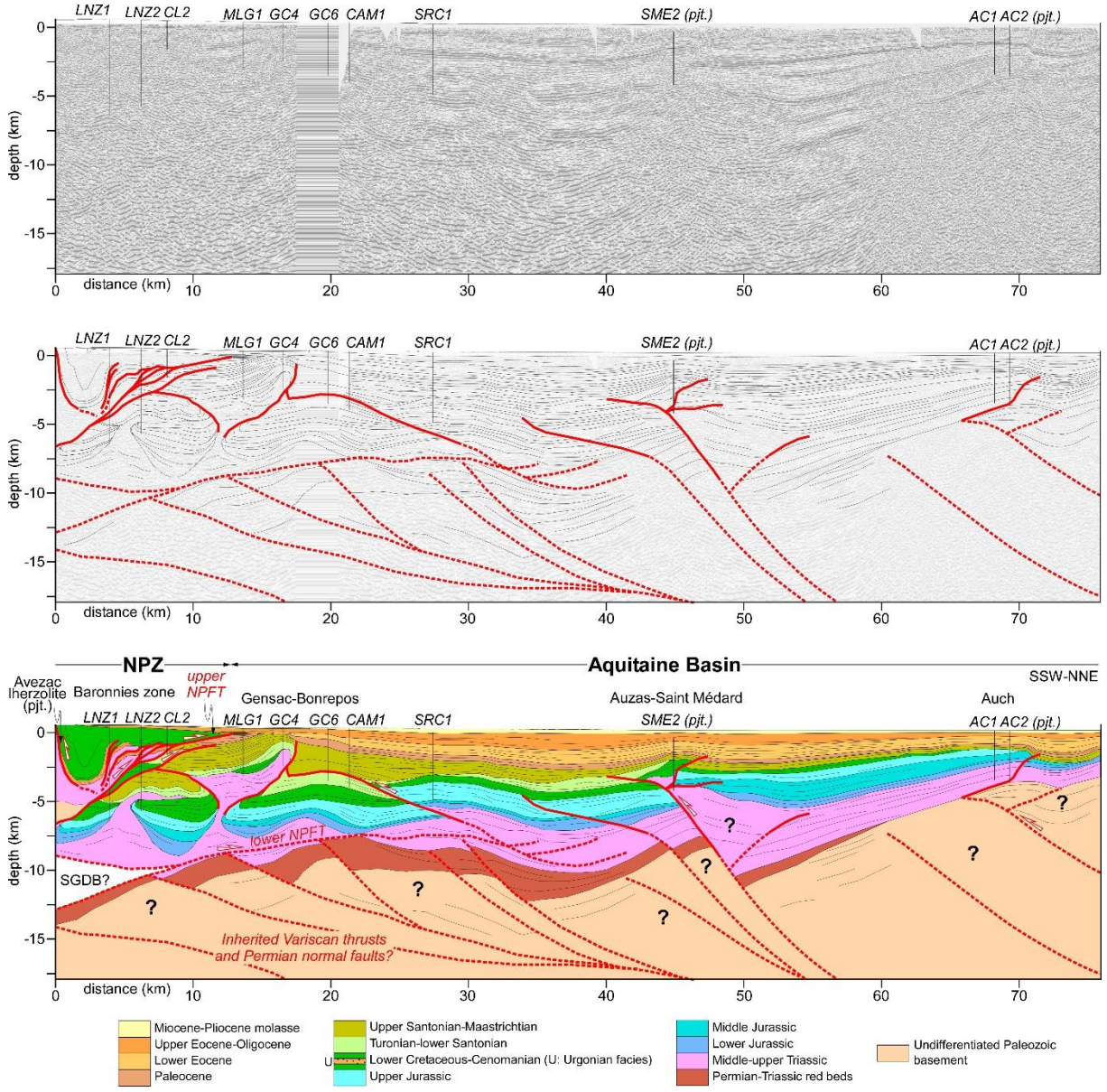

1499

1500 Figure 5

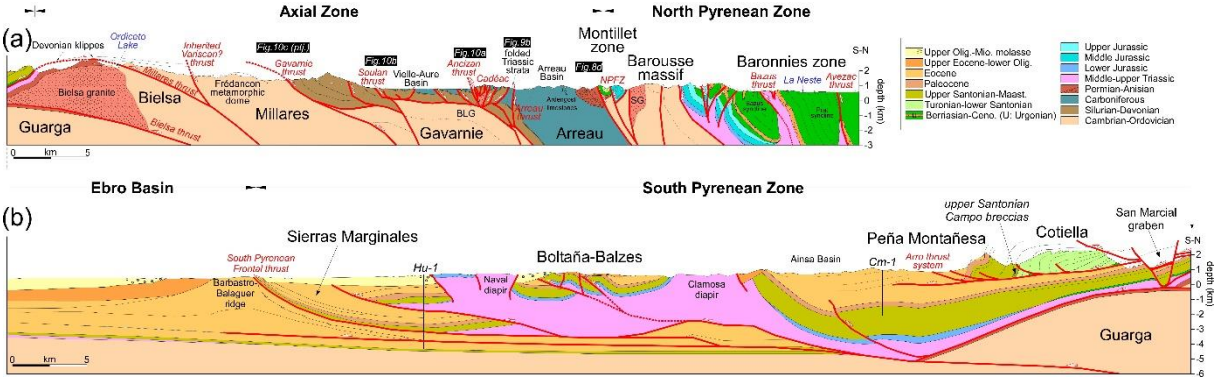

1501

1502 Figure 6

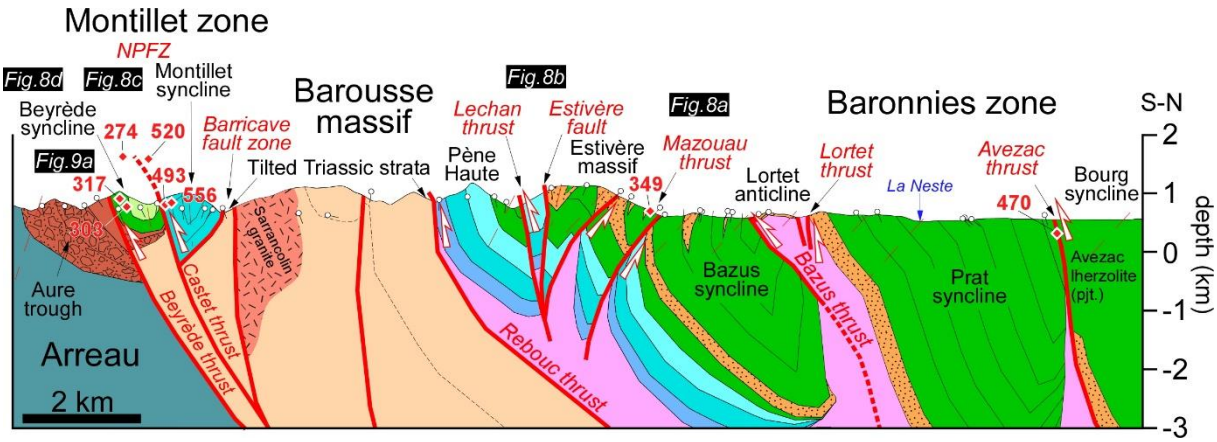

1503

1504 Figure 7

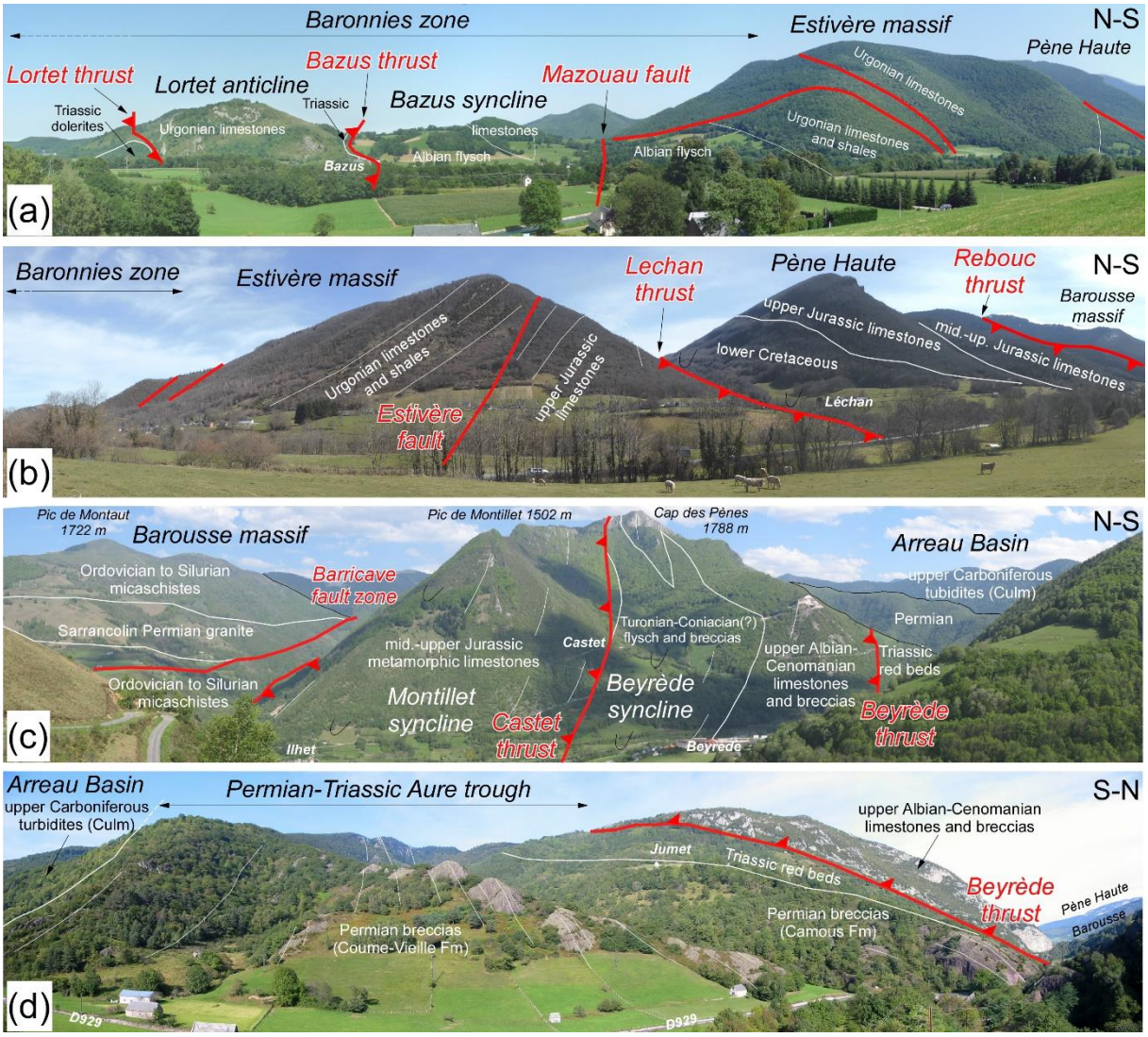

1505

1506 Figure 8

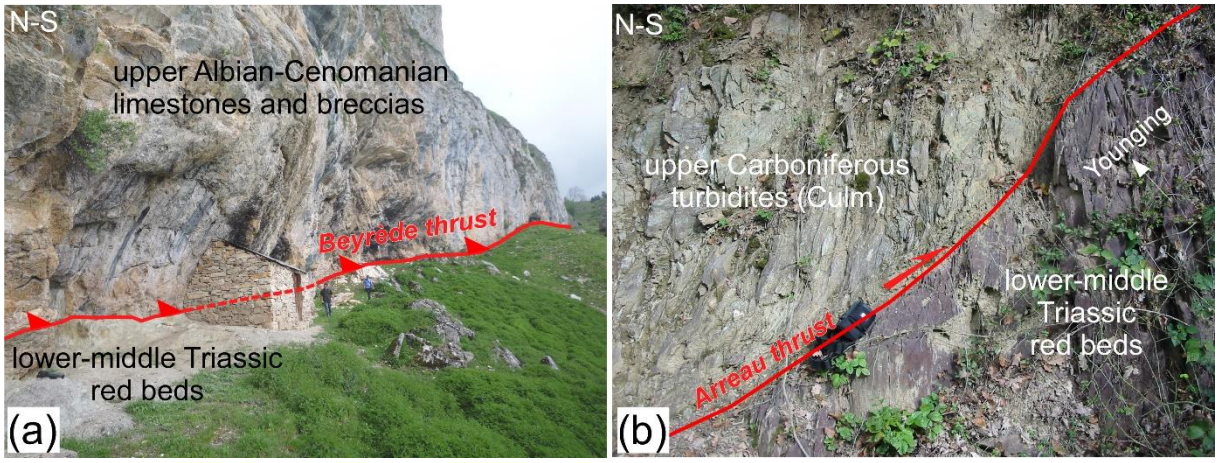

1507

1508 Figure 9

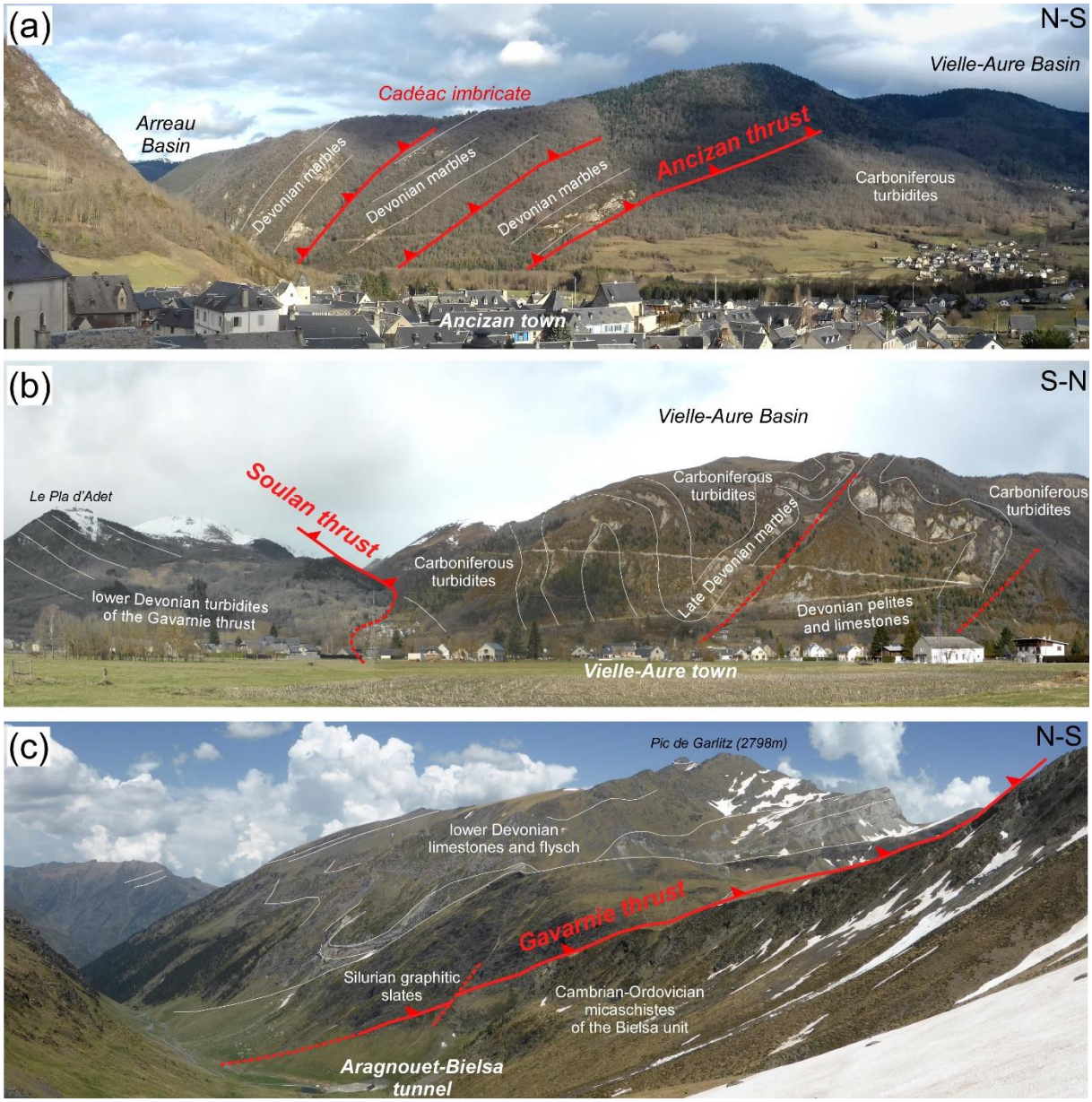

1509

1510 Figure 10

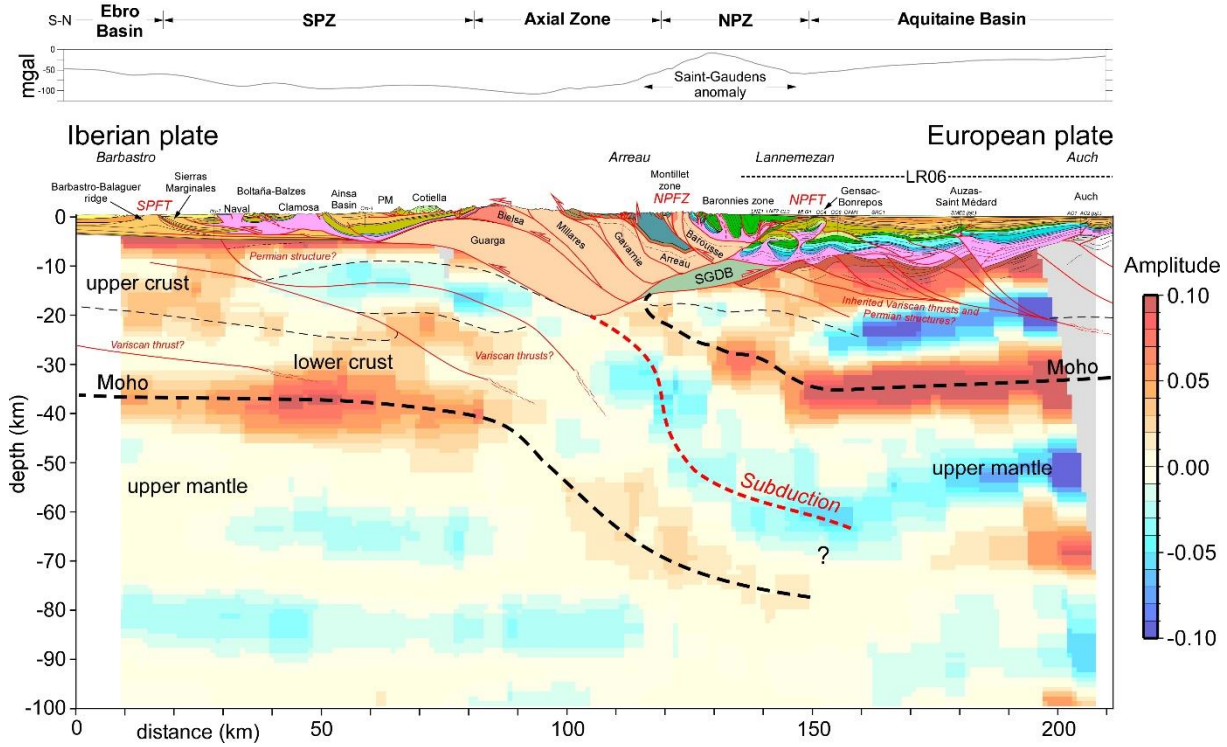

1511

1512 Figure 11

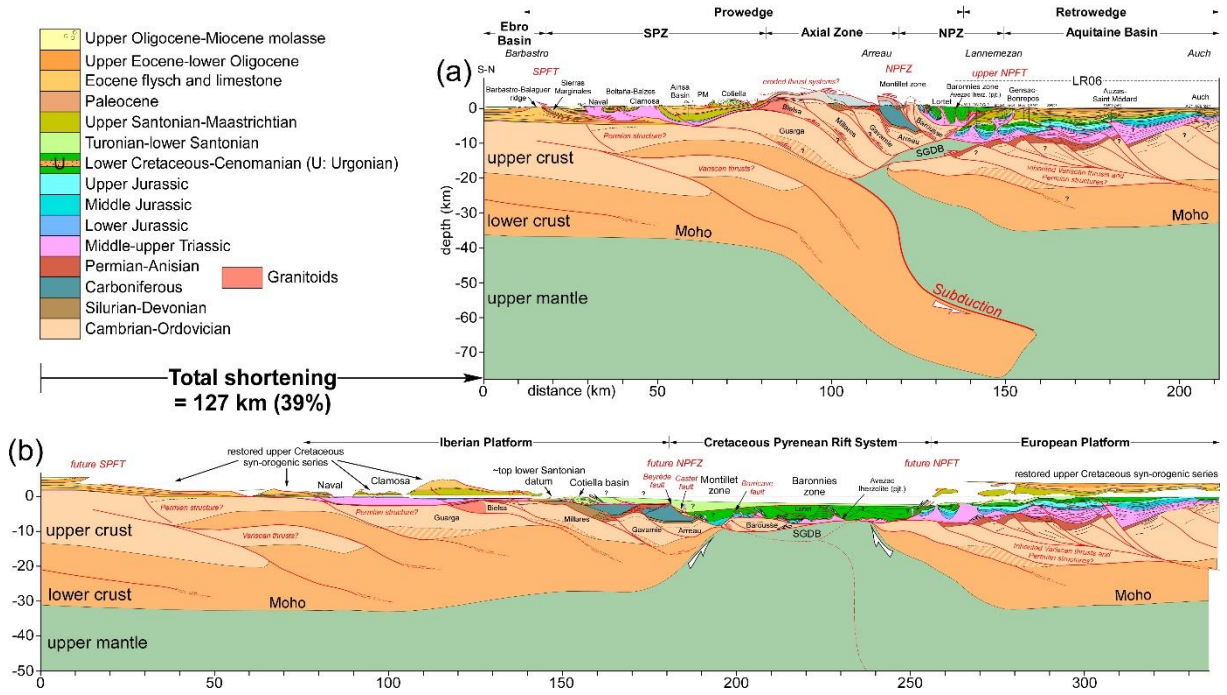

1513

1514 Figure 12

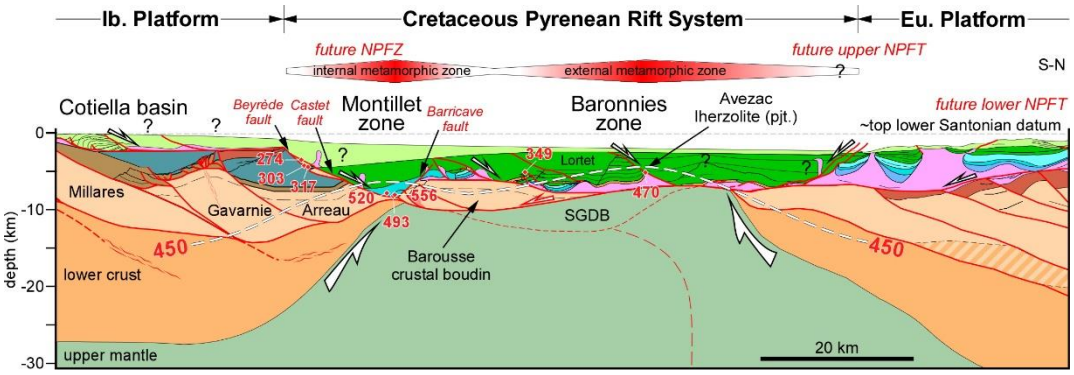

1515

1516 Figure 13

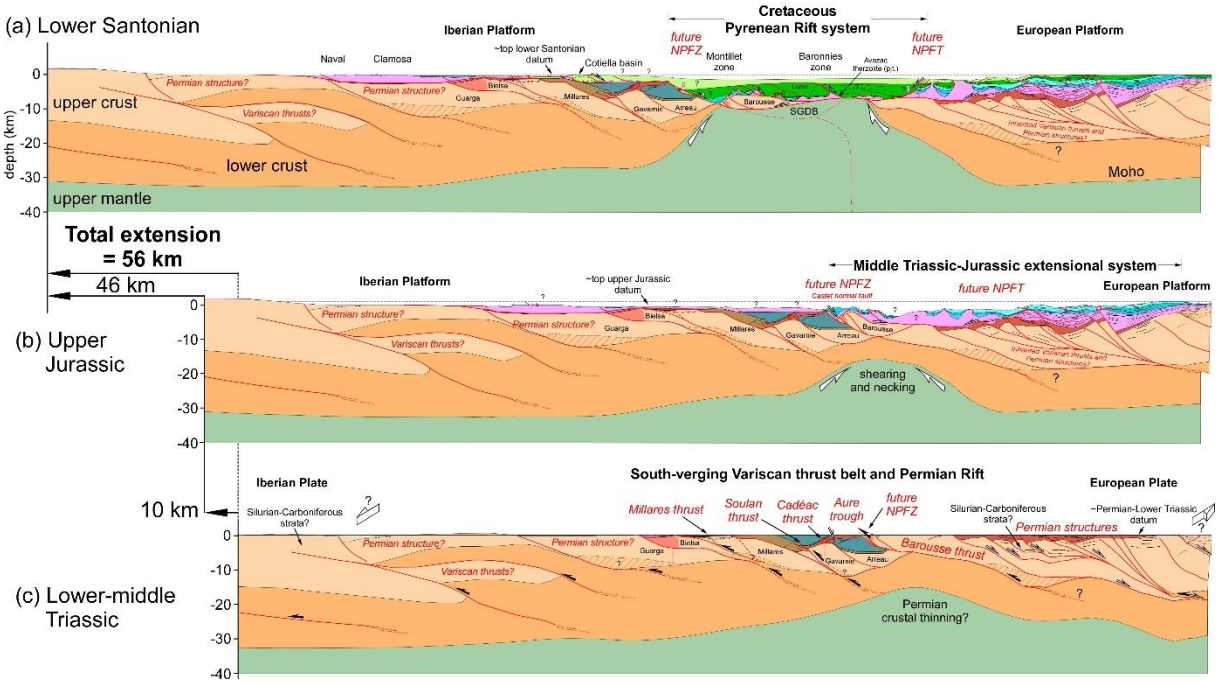

1517

1518 Figure 14

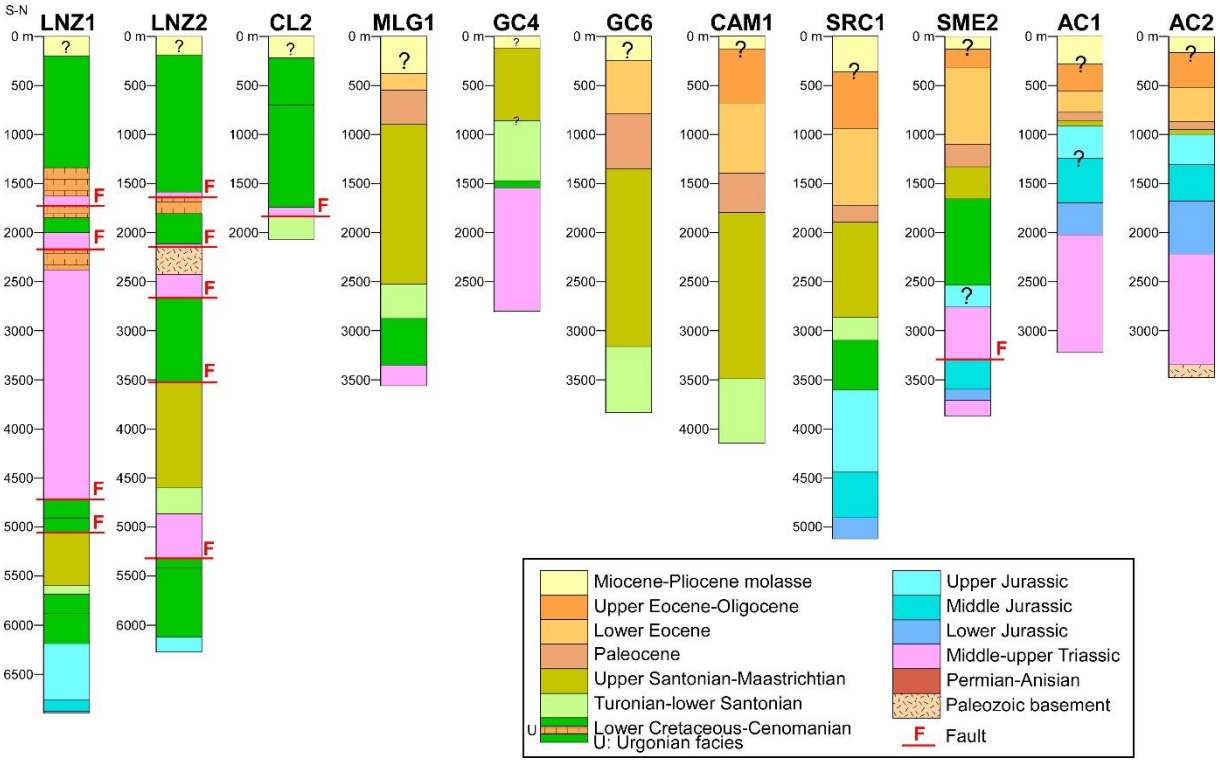

1519

1520 Figure S1